Condensin I folds the *C. elegans* genome

Moushumi Das[1,2], Jennifer I. Semple[1], Valeriia Volodkina[1,2], Anja Haemmerli[1], Janik Scotton[1], Todor Gitchev[1], Ahrmad Annan[1], Cyril Statzer[3], Collin Y. Ewald[3], Julien Mozziconacci[4], Julie Campos[1], Peter Meister[1] *

[1] Cell Fate and Nuclear Organization, Institute of Cell Biology, University of Bern, Switzerland
[2] Graduate School for Cellular and Biomedical Sciences, University of Bern, Switzerland
[3] Eidgenössische Technische Hochschule Zürich, Department of Health Sciences and Technology, Institute of Translational Medicine, Schwerzenbach-Zürich, Switzerland
[4] Laboratoire Structure et Instabilité des Génomes, UMR 7196, Muséum National d'Histoire Naturelle, 75005, Paris, France

[*] correspondence to peter.meister@unibe.ch

Abstract

Structural Maintenance of Chromosomes (SMC) complexes, cohesin and condensins, were named for their roles in meiotic and mitotic chromosome separation and compaction. Recent data from mammalian cells and *Drosophila* have described additional roles for cohesin in folding the interphase genome into loops and domains. However, determinants of genome folding in holocentric species remain unclear. Using high-resolution chromosome conformation capture, we show that *C. elegans* chromosomes exhibit two types of compartments: a large-scale compartmentalization that corresponds to central vs telomere proximal regions and a small-scale compartmentalization that reflects epigenomic states. By systematically and acutely inactivating each SMC complex, we find that in contrast to other organisms, condensin I plays a major role in long-range genome folding, while cohesin creates small loops. Loss of condensin I causes genome-wide decompaction, chromosome mixing, and disappearance of TAD structures, while reinforcing fine-scale epigenomic compartments. Counter-intuitively, the removal of condensin I and its X-specific variant condensin I^{DC} from the X chromosomes reveals the existence of a third compartment grouping together a subset of previously characterized loading sites for condensin I^{DC} and binding sites for the X-targeting complex SDC. While transcriptional changes were minor for all autosomes upon cohesin, condensin II, and condensin I/I^{DC} inactivation, removal of condensin I/I^{DC} from the X chromosome led to transcriptional up-regulation of X-linked genes. In conclusion, we describe a novel function for *C. elegans* condensin I/I^{DC} in holocentric interphase chromosome organization, which substitutes the role played by cohesin in other organisms.

Introduction

Fitting long eukaryotic genomes into the interphase nucleus requires extensive folding of the genome while maintaining the functions of replication, transcription, and repair. Chromatin conformation capture technologies and high-resolution imaging have been used to monitor genome conformation of interphase chromosomes (Dekker et al. 2002; Lieberman-Aiden et al. 2009; Cattoni et al. 2017; Stevens et al. 2017). In eukaryotes, the genome harbors a multi-layered organization, with large, multi-megabase domains named A and B-type compartments, which reflect eu- and heterochromatin, respectively (Lieberman-Aiden et al. 2009). Over shorter distances, chromosomes are folded into loops and insulated 3D domains called topologically associated domains (TADs). Over longer distances, these small scale structures are further folded to form A and B compartments. TADs serve both to restrict the action of enhancers to promoters inside the same domain and to increase enhancer-promoter contact probability, such that genes within one TAD are generally co-regulated (Lupianez et

al. 2015; Hnisz et al. 2016; Flavahan et al. 2016; Nora et al. 2012; Dixon et al. 2015). While A/B compartments correlate with the epigenetic status of the underlying chromatin, the formation of TADs is a consequence of DNA loop extrusion activities of the structural maintenance of chromosomes (SMC) complexes (Rao et al. 2017; Schwarzer et al. 2017; Wutz et al. 2017; Rosin, Nguyen, and Joyce 2018). *In vitro* and *in vivo* experiments have shown that these large ring-like complexes are able to generate loops of DNA and/or chromatin (Ganji et al. 2018; Davidson et al. 2019; Kong et al. 2020; Golfier et al. 2020).

In mammals and *Drosophila,* cohesin is the major SMC loop extruder during interphase. It interacts with oriented sequence elements bound by transcription factors like CCCTC-Binding factor (CTCF) that define boundaries between TADs as well as specific loops within TADs (Sanborn et al. 2015; Fudenberg et al. 2016; Li et al. 2020; Sexton et al. 2012). Two additional SMC complexes called condensin I and II are necessary for compaction and mechanical rigidity of mitotic chromosomes and mediate general chromosome compaction in cycling *Drosophila* cells (Yatskevich, Rhodes, and Nasmyth 2019; Rosin, Nguyen, and Joyce 2018). In mammals, condensin complexes do not appear to impact interphase chromosome folding as they are either excluded from the nucleus (condensin I) or fail to bind chromatin outside of mitosis (condensin II) (Walther et al. 2018; Abdennur et al. 2018). *C. elegans* is a notable exception to this rule as at least one condensin complex is nuclear and active during interphase.

Worms, like most metazoans, express their homologs of cohesin, condensin I and II in somatic cells (Csankovszki et al. 2009; Mito, Sugimoto, and Yamamoto 2003). Two somatic variants of the canonical cohesin complex are present and can be distinguished by their kleisin subunits, SCC-1/COH-2 and COH-1 (for a summary of the different subunits and their expression, see Haering and Gruber 2016). The different roles of cohesin^{SCC-1} and cohesin^{COH-1} are unknown at present. Worms lacking cohesin subunits or the cohesin loader show defects in rDNA compaction in embryos (Chan et al. 2003), and many cells undergo catastrophic mitoses early during embryonic development (Mito, Sugimoto, and Yamamoto 2003; Seitan et al. 2006; Wang et al. 2003). However, non-mitotic functions of cohesin during interphase remain unclear: little is known about cohesin localization on chromatin and few non-mitotic phenotypes have been described up to date.

Nematode condensin I and II are also essential for chromosome condensation during mitosis (Csankovszki et al. 2009; Ma et al. 2012; Maddox et al. 2006). Genetic deletions or RNAi knock-downs of many subunits of both condensins lead to mitotic catastrophe in early embryos, as well as nuclear defects in the few lineages that divide post-embryonically (Hagstrom et al. 2002; Stear and Roth 2002; Pasierbek et al. 2003). Additionally, a third condensin complex called condensin I^{DC} localizes specifically to the X chromosome in hermaphrodite animals during interphase. In this complex, the κ-SMC subunit SMC-4 of condensin I is replaced by its DPY-27 variant. Condensin I^{DC} is specifically targeted to the X chromosome by the Sex Determination and Dosage Compensation complex (SDC) and a sequence motif called MEX enriched on this chromosome (Meyer 2022). The binding of condensin I^{DC} in hermaphrodite animals to the X chromosome leads to the down-regulation by half of X-linked gene transcription, thereby compensating for the chromosomal imbalance between X and autosomes. Structurally, loading of condensin I^{DC} correlates with the formation of TADs and loops uniquely present on the X chromosome and not the autosomes, suggesting that at least the condensin I^{DC} variant is a *bona fide* loop extrusion factor (Crane et al. 2015; Jimenez et al. 2021; Rowley et al. 2020).

To investigate the role of the four different SMC complexes in holocentric chromosome structure in interphase, we have systematically induced cleavage of these complexes in worms and carried out phenotypic analysis, chromatin conformation capture, and RNA-seq. We show that condensin I/I^{DC} is the major determinant of chromosome folding during

interphase, while cohesin plays only a minor role. As shown for cohesin in mammals (Rao et al. 2017; Schwarzer et al. 2017), cleavage of condensin I/I^{DC} in nematodes reinforces epigenetic-driven compartments on all chromosomes and provokes the loss of TADs on the X chromosome, yet it also unexpectedly reinforces an X-specific loop compartment. At the transcriptional level, cleavage of each individual SMC complex leads to moderate changes in gene expression on autosomes. Only condensin I/I^{DC} cleavage causes major upregulation of X-linked genes. Additionally, cleavage of condensin I/I^{DC} leads to reduced animal lifespan due to its function in dosage compensation. Together, our study highlights an unexpected function of condensin I in interphase genome folding in holocentric nematodes.

Results and discussion

To interrogate the functions of SMC complexes, we constructed strains in which individual complexes can be removed from chromatin by cleaving the kleisin subunit by heat-shock induced expression of the Tobacco Etch Virus (TEV) protease (Fig. 1A; Uhlmann, Lottspeich, and Nasmyth 1999). We modified the endogenous genes for the two somatic kleisins of cohesin *coh-1* and *scc-1* (also known as *coh-2*), as well as *dpy-26* and *kle-2*, generating TEV-cleavable cohesins (with COH-1 or SCC-1), condensin I/I^{DC} and condensin II, respectively. Under non-heat-shock growth conditions, TEV cut sites in kleisins were readily tolerated by the animals and generated no obvious phenotypes.

Cohesin and Condensin II cleavage impairs vulval development

To first analyze the mitotic functions of SMC complexes, we induced kleisin cleavage in the first larval stage and scored the phenotypic consequences on late-stage development (Fig. 1B). At this point, 90% of all cells are post-mitotic, except for the hypodermal/seam lineages, the somatic gonad, and the ventral hypodermal cells which give rise to the vulva, a non-essential organ that allows egg-laying (Sulston and Horvitz 1977). Expression of TEV in otherwise wild-type worms had no effect, while cohesin^{SCC-1} cleavage had strong phenotypic consequences, notably developmental delay, morphological changes, and a variety of phenotypes linked to a non-functional vulva (64% of the animals, Fig. 1B, S1). Since most cells are post-mitotic, these results suggest that cohesin^{SCC-1} cleavage interferes with mitosis and/or terminal differentiation of the vulval precursor cells. In contrast, cleavage of cohesin^{COH-1} had no phenotype, with all animals eventually growing into egg-laying adults. Simultaneous cleavage of cohesin^{SCC-1} and cohesin^{COH-1} led to similar phenotypes as those observed for cohesin^{SCC-1} with a higher penetrance, suggesting on the one hand minor roles for cohesin^{COH-1} and on the other hand a partial overlap of mitotic functions between the two cohesin variants.

In contrast to cohesin^{SCC-1} cleavage, cleavage of condensin I/I^{DC} or condensin II independently only slightly delayed late-stage development. Most worms (>90%) eventually developed into egg-laying adults and showed no other phenotype. Following simultaneous cleavage of both condensins, however, a large majority of the animals displayed phenotypes linked to aberrant vulval development (Fig. 1B). This demonstrates that condensin I/I^{DC} and II can complement each other's functions, yet at least one condensin type is necessary for post-embryonic development. This absence of phenotype in slowly dividing cells is reminiscent of the subtle changes observed in mammalian cells upon individual condensin subunit depletion (Hirota et al. 2004; Gerlich et al. 2006): in cultured cells, the depletion of condensin I or II subunits changes the mechanical rigidity of the mitotic chromatids and delays chromosome condensation during early prophase but does not impair mitotic progression.

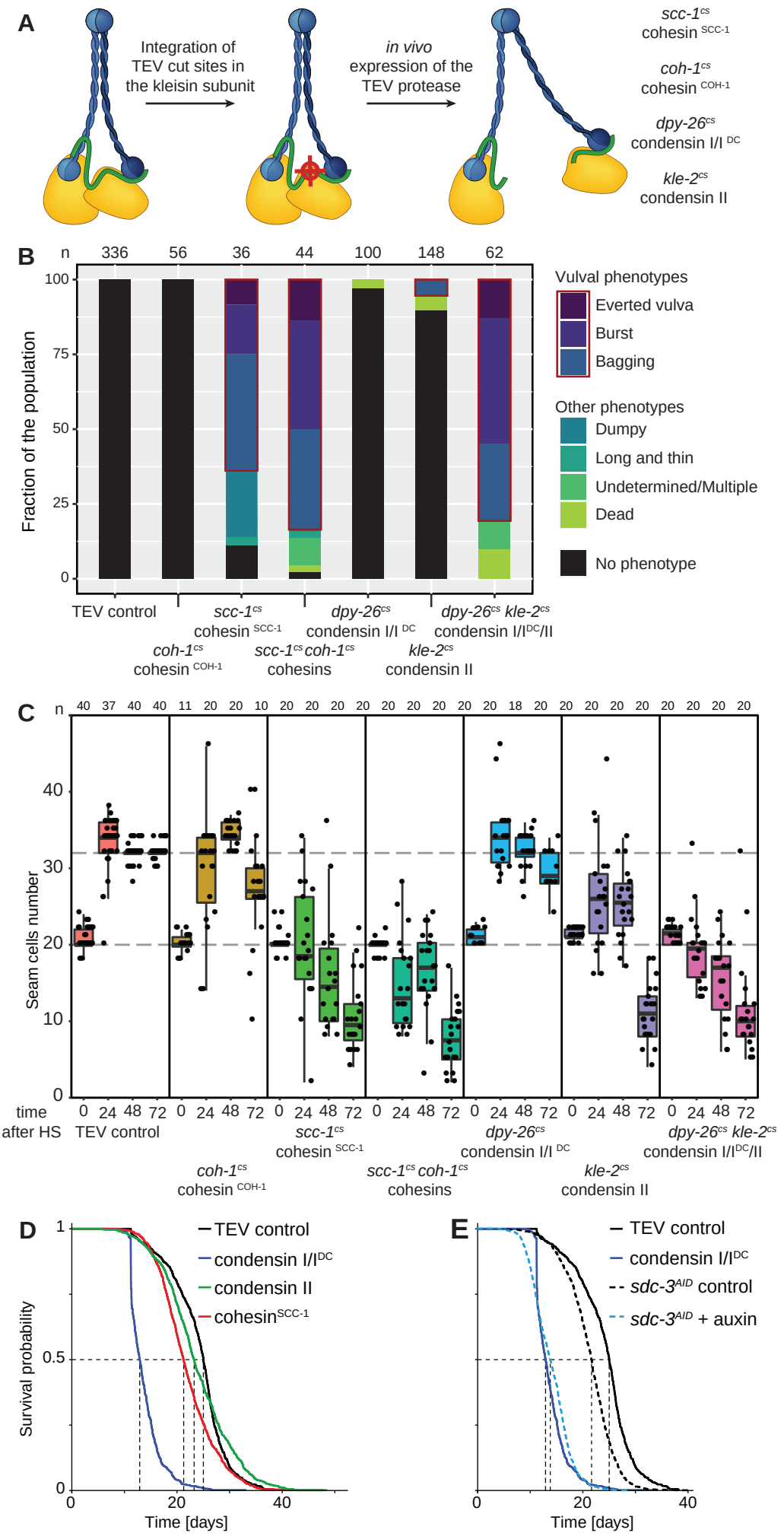
A
Integration of TEV cut sites in the kleisin subunit
in vivo expression of the TEV protease
scc-1cs cohesin SCC-1
coh-1cs cohesin COH-1
dpy-26cs condensin I/I DC
kle-2cs condensin II
B
n 336 56 36 44 100 148 62
Fraction of the population
Vulval phenotypes
Everted vulva
Burst
Bagging
Other phenotypes
Dumpy
Long and thin
Undetermined/Multiple
Dead
No phenotype
TEV control
coh-1cs cohesin COH-1
scc-1cs cohesin SCC-1
scc-1cs coh-1cs cohesins
dpy-26cs condensin I/I DC
kle-2cs condensin II
dpy-26cs kle-2cs condensin I/IDC/II
C
n 40 37 40 40 11 20 20 10 20 20 20 20 20 20 20 20 20 18 20 20 20 20 20 20 20 20
Seam cells number
time after HS
0 24 48 72
TEV control
coh-1cs cohesin COH-1
scc-1cs cohesin SCC-1
scc-1cs coh-1cs cohesins
dpy-26cs condensin I/I DC
kle-2cs condensin II
dpy-26cs kle-2cs condensin I/IDC/II
D
Survival probability
Time [days]
TEV control
condensin I/IDC
condensin II
cohesinSCC-1
E
TEV control
condensin I/IDC
sdc-3AID control
sdc-3AID + auxin
Time [days]

Figure 1 - Loss of cohesin^{SCC-1} and condensin II causes disruption in post-embryonic vulval development and seam cell progression. A. Experimental approach for the functional analysis of SMC complexes *in vivo*. Adapted from (Haering and Gruber 2016). **B.** Phenotypic outcome 72 hours post-induction of individual kleisins cleavage for the indicated SMC complexes (condensin I/I^{DC}, condensin II, cohesin^{SCC-1} and cohesin^{COH-1}) and multiple SMC complexes (cohesin$^{SCC-1\ COH-1}$ and condensin I/I^{DC}/II). TEV control corresponds to a strain in which only the protease is expressed without any target cut site insertion. **C.** Seam cells count per animal each day after kleisin cleavage induction of indicated SMC complexes. **D.** Lifespan analysis of animals after cleavage of the different indicated SMC complexes. Animals were transferred on day 1 of adulthood to plates with FUdR and scored automatically in the lifespan machine (Stroustrup et al. 2013). **E.** Lifespan analysis of animals upon auxin-mediated degradation of the condensin I^{DC} loader SDC-3, comparing animals with and without auxin. TEV control and condensin I/I^{DC} as in D. for the sake of comparison.

Consequences of kleisin cleavage for seam cells divisions

To further characterize the roles of SMC complexes in mitosis, we analyzed seam cell divisions after kleisin cleavage in L1 larvae, as these can be followed *in vivo* by the expression of specific fluorescent markers (Koh and Rothman 2001). Cell division in this lineage is stereotypic and entails one asymmetric cell division per larval stage, giving rise to one seam cell and one hypodermal cell which fuses with the rest of the hypoderm (Sulston and Horvitz 1977; Singh and Sulston 1978). Thus, the number of seam cells remains constant, except for a symmetric division during larval stage 2, which leads to an increase from 20 to 32 seam cells (see TEV control animals, Fig. 1C). Wild-type numbers of cells were obtained after cleavage of cohesin^{COH-1}, while the cleavage of cohesin^{SCC-1} led to a decrease to less than 20 seam cells. Cleavage of both cohesin kleisins SCC-1 and COH-1 had additive effects, with a more severe decrease in seam cell numbers and misalignment of the cells along the longitudinal axis of the body. The additive effect confirms that cohesin^{SCC-1} is the major mitotic cohesin in post-L1 larvae, and its loss alters both the integrity and the orientation of the mitotic plane. Surprisingly, and in contrast to RNAi studies against individual subunits of condensin I/I^{DC} (Csankovszki et al. 2009), cleavage of the condensin I/I^{DC} had no effect on seam cell numbers, suggesting seam cell mitosis progressed faithfully in the latter's absence. This was not the case for cleavage of condensin II, which led to a reduction in the number of seam cells to less than 20 cells within 48 hours as well as mitotic axes misalignment (Fig. 1C). Cleavage of both condensins led to a more rapid but similar decrease in seam cell number, reminiscent of the one observed upon cleavage of both cohesins (Fig. 1C). Together with the phenotypic analysis, we conclude that condensin II and cohesin^{SCC-1} are necessary for post-embryonic cellular divisions while condensin I/I^{DC} and cohesin^{COH-1} cleavage are not.

Cleavage of Condensin I/I^{DC}, but not Condensin II or Cohesin drastically reduces lifespan

To evaluate the physiological impact of cohesin and condensin cleavage at the organismal level, we measured animal lifespan after kleisin cleavage using automated lifespan analysis. Lifespans are carried out on FUdR that impairs embryonic development *in utero*, therefore issues with non-functional vulva are avoided. Cleavage of condensin II or the major cohesin^{SCC-1} consequently had little impact: animals lived almost as long as TEV control animals (Fig. 1D). By contrast, cleavage of condensin I/I^{DC} caused a drastic reduction in lifespan as most animals were dead by day 15, while only 3% were still alive by day 20, compared to 71% of TEV control animals alive by day 20 (Fig. 1D). As no mitotic phenotype (see above) could be observed in animals upon cleavage of condensin I/I^{DC} only, the reduction of lifespan is, therefore, most likely a consequence of the non-mitotic functions of this SMC complex.

Hereafter, we first describe HiC data in control animals before interrogating the impact of individual SMC cleavage on chromatin folding.

HiC analysis identifies genome organization at different scales

We performed high-resolution chromosome conformation capture (HiC) in third larval stage animals, in wild-type N2 and TEV control animals (Fig. 2AB, S2A, S3). As observed previously, the autosomes in control animals do not display the TAD structure observed in most metazoans, but are segmented in three large contact domains (Fig. 2A): two large multi-megabase domains located on the distal ends of the chromosomes (hereafter called T domains for telomere-proximal, corresponding to chromosomal arms) and a large domain located in the chromosome center (C domain). This correlates with the spatial segregation of repeat-rich heterochromatic T domains at the nuclear periphery and the transcriptionally more active C domain located inside the nuclear lumen (Ω shape, for review see Sharma and Meister 2013). This chromosome organization has been described at the single-cell level in embryonic blastomeres using chromosome tracing techniques (Sawh et al. 2020). Perinuclear anchoring depends largely, at least in embryonic stages, on H3K9 methylation marks enriched on chromosomal arms and the anchoring of these regions to the nuclear periphery *via* CEC-4, a chromodomain protein embedded in the nuclear envelope (E. C. Anderson, Yang, and Meyer 2020; Towbin et al. 2012; Gonzalez-Sandoval et al. 2015). Genome-wide HiC contact matrices highlight this long-range organization in *cis* and *trans* (Fig. 2AC, TEV control, S2A). Additionally, a clear cross-hatched pattern is observed at a small scale (2-40kb, Fig. 2AG, TEV control), both in *cis* and *trans*, indicating the presence of smaller compartments embedded into the T and C large domains (Fig. 2A, TEV control, S2A). Eigenvectors of the HiC matrix reflect this two-tiered organization (Fig. 2A bottom, S2A): the first eigenvector delineates large scale T/C domains while the second one captures intra-chromosomal compartments and the weaker inter-chromosomal small-scale cross-hatch pattern (Fig. 2A, S2A).

Both large domains and small compartments correlate with transcription, yet we observe a far better correlation for small compartments (Fig. 2C). A comparison of eigenvector values with previously characterized chromatin states confirmed this correlation with transcriptional activity (Fig. 2D, S2C, Evans et al. 2016). T domains are enriched for H3K9 methylated chromatin, but a significant portion bears active histone marks as transcriptionally active genes within T domains are found interspersed among silent repeats. Conversely, C domains are enriched for active states, yet also harbor many Polycomb-marked regions (Fig. 2D, S2B). In contrast, small compartments faithfully separate active and silent chromatin: small compartments with high second eigenvector values are highly enriched for active chromatin states, while the ones with low values harbor inactive states, including both H3K9 and H3K27 methylation. These small compartments are therefore similar to A and B-type chromatin compartments previously described in mammalian systems, although they are much smaller in size (Lieberman-Aiden et al. 2009). Similar small A and B-type compartments have been described in nematodes using DNaseI HiC (ARC-C) and have been suggested to represent a TAD-like structure (Huang et al. 2021). Indeed, pileup analysis of large (>10kB) A and B-type compartments highlighted insulated domains (Fig. S2C) and the aggregated insulation score between A and B domains showed a minimum at the boundary (Fig. S2CD). Our analysis, therefore, reveals that these small compartments correlate with epigenomic states as previously described in mammalian cells and *Drosophila* (Nuebler et al. 2018; Lieberman-Aiden et al. 2009). Interestingly, and in contrast to active and silent chromatin states, regions labeled as “mixed, tissue-specific” are distributed across all A/B small compartments eigenvalues except very high ones (Fig. 2D). Given that HiC is performed on whole animals that contain a diversity of cell types, we conclude that the global genome folding (*i.e.* T *vs* C) is similar between cells, while tissue-specific genes join the A or B compartments depending on their cell-type-specific chromatin state (Meister et al. 2010). In summary, we find that two overlapping levels direct worm genome folding: first, confirming earlier studies, repeat-rich, mainly heterochromatic outer thirds of chromosome arms of autosomes form large T perinuclear domains (Towbin et al. 2012; Liu et al. 2011; Ikegami et al. 2010; Gonzalez-

Aguilera et al. 2014; Bian et al. 2020), while the central sections of autosomes, transcriptionally more active, are located in the nuclear lumen (large C domains). Second, small regions preferentially interact together based on their transcriptional status and epigenomic marks to form distinct small A and B compartments as in mammalian and *Drosophila* genomes.

In contrast to autosomes, the X chromosomes in hermaphrodite worms are unique in that they fold into megabase-sized TADs created by the activity of the X-specific putative loop extrusion factor condensin I^{DC} (Crane et al. 2015; Jimenez et al. 2021; Brejc et al. 2017; Erika C. Anderson et al. 2019). X chromosomes lie mostly in the large C domain (data not shown), yet small compartments within the large X chromosome TADs form a cross-hatched pattern that, as for autosomes, correlates with chromatin states (Fig. S2B). Additionally, high contact probability signals located at the corners of the TADs indicate the presence of stable loops between TAD boundaries (Fig. 2B, TEV control). These loops have been observed previously in HiChIP experiments with the condensin I^{DC} subunit DPY-27, and can span over two or more of the TAD boundary elements defined at the sequence level by the strong Motif Enriched on X (MEX) motifs (Albritton et al. 2017; Rowley et al. 2020).

Condensin I/I^{DC} is the major SMC complex for interphase genome folding

In mammalian cells, cohesin is involved in interphase chromosome folding besides its role in mitosis (Wutz et al. 2017; Schwarzer et al. 2017; Rao et al. 2017). Cohesin extrudes DNA loops, and this activity is blocked at oriented boundary sequence elements recognized by the Zn-finger DNA binding factor CTCF (Davidson et al. 2019; Fudenberg et al. 2016; Li et al. 2020). In nematodes, it is unclear which SMC complex, if any, drives loop formation on interphase autosomes.

We, therefore, examined the role of SMC complexes by performing HiC following individual kleisin cleavage of cohesins or condensins. In contrast to mammals, for which cohesin depletion or ablation leads to a sharp decrease in contact probabilities (Wutz et al. 2017; Schwarzer et al. 2017; Rao et al. 2017), cleavage of either of the two worm cohesins decreased only mildly the contact probabilities at short distances (10-100 kb, Fig. 2EF, S2H). This limited decrease was larger for $cohesin^{SCC-1}$ cleavage than for $cohesin^{COH-1}$ (Fig. 2F, S2H inset). Condensin II cleavage had no effect on chromosome folding, implying that its function is largely to ensure mitotic chromosome compaction (Fig. S2EF). In contrast, condensin I/I^{DC} cleavage led to major changes in contact frequency maps. At short distances (<100 kb, Fig. 2EF,S2G), the contact probabilities were identical to the control. For larger distances (>100 kb - 3 Mb), contact probabilities decreased as compared to the control. Condensin I/I^{DC} therefore appears to promote long-range (>100 kb) contacts, as in fission yeast (Kakui et al. 2020). At distances larger than 3 Mb, contact probability was higher after condensin I/I^{DC} cleavage than in control experiments or cleavage of other SMC complexes (Fig. 2F), suggesting that these very long-range contacts are repressed by condensin I/I^{DC} action. Similarly, *trans* chromosome contacts were markedly increased for all chromosomes upon condensin I/I^{DC} cleavage, which was not the case for cleavage of any other SMC complex (Fig. 2E). Similar chromosome mixing has been observed previously in *S. pombe* condensin mutants, but not upon acute depletion of the SMC subunit Cut14 (Kakui et al. 2020; Iwasaki, Corcoran, and Noma 2016). These data strongly suggest that condensin I/I^{DC} is the major loop extrusion factor that folds the interphase genome in nematodes.

By analogy with observations made in mammalian cells upon depletion of cohesin, one would predict that a consequence of condensin I/I^{DC} cleavage would be the reinforcement of A and B compartments (Schwarzer et al. 2017; Rao et al. 2017). Indeed, condensin I/I^{DC} cleavage (but no other kleisin cleavage) led to an increase of contact frequency in the checkerboard and cross-hatch patterns at large and small scales, respectively (Fig. 2AB, compare TEV control to condensin I/I^{DC} cleavage, 2EG). Inside individual chromosomes, T and C domains

were reinforced as well as small B compartments. Between chromosomes, the contact probability between autosomal central C domains increased the most, as well as between small B compartments (Fig. 2EG). On top of being reinforced, the average size of small A and B compartments increased by 62% and 54%, respectively (Fig. 2H). An exception to this rule was chromosome X, for which the entire chromosome showed an increase of *trans* contact probability with the T domains of each autosome (Fig. 2E). As the T regions are located at the nuclear periphery, this strongly suggests a relocation of the X chromosome towards the nuclear periphery upon condensin I/I^{DC} cleavage as previously observed (Sharma et al. 2014).

We next analyzed genomic regions which switch compartments, by dividing the small A/B compartment track into equally-sized groups (terciles; high (H), middle (M), and low(L)) and monitoring regions switching from one tercile to another upon kleisin cleavage. For all kleisins, very few regions shifted more than one tercile upon cleavage. Most changes were observed upon condensin I/I^{DC} cleavage, for which 21% of bins switched terciles (versus 8-12% for other kleisins). Bins switching down from H to M or M to L showed depletion for annotated transposable elements, enrichment for annotated non-coding RNAs and tRNAs, active histone marks, and increased gene expression upon cleavage, compared to bins switching up from M to H or L to M (Fig. S4). Chromatin states annotated as introns and repeats were similarly under-represented in bins switching down from H to M or M to L compared to bins switching in the reverse direction.

Together, we conclude that the main SMC complex involved in chromosome folding in *C. elegans* is condensin I/I^{DC}, while cohesin is involved in short-range looping. Cleavage of condensin I/I^{DC} on the one hand leads to extended genome decompaction and increased *trans* chromosomal contacts, and on the other hand to increased epigenomic compartmentation. Why would condensin I in worms take the role of cohesin in mammals? In mammals, most cohesins are removed from chromosome arms shortly before anaphase while centromeric complexes ensure sister chromatid cohesion (for review, Yatskevich, Rhodes, and Nasmyth 2019). Repurposing condensin I for genome folding might be linked to the holocentric nature of chromosomes in nematodes. In worms, centromeres are defined by the binding of transcription factors and active transcription, thereby differentiating between centromeric and non-centromeric cohesin populations becomes difficult (Steiner and Henikoff 2014). Using condensin I/I^{DC} as an alternative loop extruder would functionally separate SMC complexes involved in sister chromatid cohesion from the ones involved in interphasic genome looping. Noticeably, nematodes have no CTCF - involved in TAD boundary formation in mammals - suggesting that the genome folding relies mainly on T/C domains and the small epigenomic A/B compartments, rather than TADs. The absence of TAD structure in the sense of an extrusion domain limited by sequence elements also suggests that transcriptional regulation in nematodes is carried out by proximal enhancers located close to their target promoters. Indeed, the compendium of enhancer sequences shown to be able to activate transcription of reporter genes are all located within 5 kb from their putative target gene (Jänes et al. 2018; Daugherty et al. 2017). This is in stark contrast to gene regulation in mammalian cells, for which enhancers can be located megabases away from their target gene, but for which TAD structure limits their activation potential (Zuin et al. 2021).

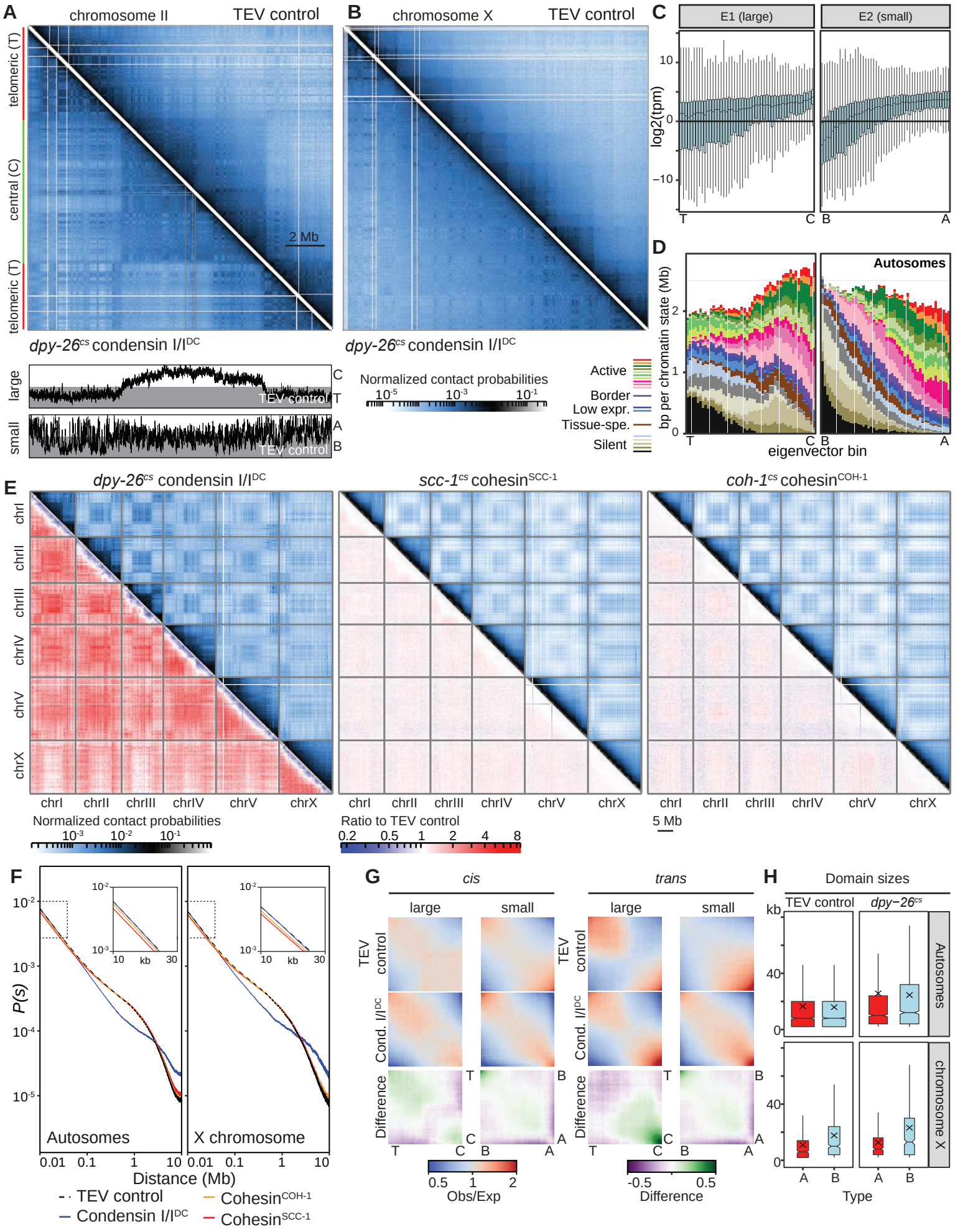
A
chromosome II
TEV control
telomeric (T)
central (C)
telomeric (T)
2 Mb
dpy-26cs condensin I/IDC
large
small
TEV control
TEV control
B
chromosome X
TEV control
dpy-26cs condensin I/IDC
Normalized contact probabilities
10-5 10-3 10-1
C
E1 (large)
E2 (small)
log2(tpm)
10
0
−10
T C B A
D
Autosomes
bp per chromatin state (Mb)
2
1
0
T C B A
eigenvector bin
Active
Border
Low expr.
Tissue-spe.
Silent
E
dpy-26cs condensin I/IDC
scc-1cs cohesinSCC-1
coh-1cs cohesinCOH-1
chrI chrII chrIII chrIV chrV chrX
Normalized contact probabilities
10-3 10-2 10-1
Ratio to TEV control
0.2 0.5 1 2 4 8
5 Mb
F
P(s)
10-2
10-3
10-4
10-5
Autosomes
X chromosome
10 kb 30
0.01 0.1 1 10
Distance (Mb)
TEV control
Condensin I/IDC
CohesinCOH-1
CohesinSCC-1
G
cis
trans
large
small
TEV control
Cond. I/IDC
Difference
T C B A
0.5 1 2
Obs/Exp
-0.5 0.5
Difference
H
Domain sizes
TEV control
dpy−26cs
kb
40
0
Autosomes
chromosome X
A B A B
Type

Figure 2 - Condensin I folds the *C.elegans* interphase genome. A. HiC contact frequency matrices for chromosome II in TEV control animals (top right) and upon condensin I/I^{DC} cleavage (bottom left). The compartment tracks at the bottom show the first and second *trans* eigenvectors of the genome-wide TEV control matrices, with large, megabases size telomeric and central (T/C) domains identified in the first one, and small tens of kb-sized A/B compartments identified on the second one. **B.** X chromosome HiC contact frequency matrices for TEV control (top right) and upon cleavage of condensin I/I^{DC} (bottom left). **C.** Correlation of first (E1, large) and second (E2, small) eigenvectors values with transcription in TEV control animals. Eigenvector values for 2 kb genomic regions were binned into 50 equally-spaced intervals and expression values were determined for each bin. Spearman correlation of RNA-seq tpm *vs* eigenvalues in all autosomal 2 kb bins: 0.25 for large domains and 0.4 for small compartments. **D.** Chromatin state composition of eigenvector bins. The chromatin state composition of each chromosome interval as measured by (Evans et al. 2016) was correlated with the first (large T/C domains) and second (small A/B compartments) eigenvector value of each interval for autosomes. Similar results for the X chromosome and detailed chromatin states description are shown in Fig. S2. **E.** Top right triangles: genome-wide HiC contact frequency maps in L3 animals following cleavage of the indicated SMCs. Bottom left triangles: Ratio to TEV control of the indicated kleisin cleavage. Pooled data from two biological replicates per condition. **F.** Contact probability decay plots for pooled autosomes and the X chromosome after kleisin cleavage of the different SMC complexes. Inset: short distance contact probability decay plot for the same conditions. **G.** Saddle contact probability plots for large T/C domains and small A/B compartments in *cis* (left) and *trans* (right) in TEV control (upper row), and in animals after condensin I/I^{DC} cleavage (middle row). Difference between the two conditions is shown in the bottom row. **H.** A and B compartment sizes on autosomes and the X chromosome in TEV control and upon condensin I/I^{DC} cleavage (*dpy-26^{cs})*. The cross and the horizontal midline of the box denote the mean and median domain sizes, respectively, the box outlines values between the first and third quartile.

Condensin I/I^{DC} cleavage leads to X chromosome TAD disappearance and reinforcement of an X-specific loop compartment

In mammalian cells, loss of cohesin leads to the disappearance of TADs and loops (Wutz et al. 2017; Schwarzer et al. 2017; Rao et al. 2017). As these structures are only present on the X chromosome in *C. elegans*, we asked how cleavage of the different SMC complexes impact on the latter. Similar to autosomes, cleavage of either cohesin kleisins led to a slight loss of contact probability at short distances (10-100 kb) while condensin II cleavage had no effect (Fig. 2F,S2H). Condensin I/I^{DC} cleavage led to major changes at a large scale (>100 kb, Fig. 2B lower panel): X-specific TADs were no longer visible and insulation between TADs was either lost or greatly weakened (Fig. 2B,3ABD,4A). Cleavage of the putative loop extruder condensin I/I^{DC} did however not lead to the loss of the spots located at the TAD corners, indicative of stable loops. On the contrary, thirty-seven small regions showed increased reciprocal contact frequencies, for some across several megabases, creating dotted lines on the HiC contact probability map (Fig. 3A). Manual mapping and automatic detection using Mustache of the loops or their anchors showed a high overlap between loop anchors and TAD boundaries seen in wild-type and TEV control animals (Fig. 3AB, Roayaei Ardakany et al. 2020). While each anchor would create contacts with a limited number of neighboring boundaries in control situations (median 6, Fig. 3F), cleavage of condensin I/I^{DC} led to an increase in the number of loops per anchor (median 19, Fig. 3F). Additionally, the mean size of loops increased from 1.25 Mb in the control animals, to 3.7 Mb upon condensin I/I^{DC} cleavage, and many loops had sizes larger than 8 Mb, which represents half the entire X chromosome length (Fig. 3F). Aggregated peak analysis (APA) using all possible loops defined by the reciprocal contacts between anchors confirmed that contact frequencies between anchors increased both at small (<5Mb; 30% increase relative to background) and large scale (5-17 Mb; 80% increase; Fig. 3E). MEME motif detection identified the MEX motif in thirty-five out of thirty-seven loop anchors and 32 out of 37 co-localized with previously identified *rex* sites, a subset of MEX motifs with high enrichment for the X-specific complex condensin I^{DC} targeting complex (Fig. 3A, bottom) (Albritton et al. 2017). Additionally, using a previous classification of *rex* sites based on ChIP-seq enrichment for condensin I^{DC} and the putative loading complex SDC-2 as strong, intermediate and weak *rex (Albritton et al. 2017),* we observed that 15 out of 17 (88%) strong *rex* sites overlap with loop anchors. Only half (8 out of 16) and 9 out of 31 (29%) intermediate and weak strength *rex* sites overlap with anchors, respectively. Consequently, comparison with ChIP-seq data demonstrated high and correlated enrichment of loop anchors for condensin I^{DC} and the X-specific targeting complex subunits

SDC-2, SDC-3 and DPY-30 (Fig. 3G). Loop anchors colocalized with a subset of the highest ChIP peaks for these proteins, but not all peaks, with an average enrichment between 44 and 157 times higher than the average enrichment in the surrounding 100 kb regions (Fig. 3G). Surprisingly, the other SMC complexes cohesin^{SCC-1} and condensin II showed a similar enrichment at loop anchors, suggesting that the anchors are boundary elements for all SMC complexes.

A similar reinforcement of corner peaks located at TAD boundaries has been observed previously in mammalian cells at CTCF binding sites upon knock-down of the cohesin destabilizer WAPL or protection from WAPL by acetylation of cohesin^{STAG1} (Wutz et al. 2020; Haarhuis et al. 2017). Mechanistically, long-range loop extrusion was proposed to lead to these horizontal and vertical dotted lines. However, whereas in these studies the loop extruders are stabilized onto chromatin, our experiments release the putative loop extruders condensin I/I^{DC} from chromatin. One might suggest that removal of condensin I/I^{DC} leads to stabilization of other loop extruders such as cohesin, which would normally be displaced by condensin I/I^{DC}. A consequence of this hypothesis would be the accumulation of cohesin following condensin I/I^{DC} cleavage into microscopically visible spots. We did not observe such clusters using a fluorescently tagged SMC-1 shared cohesin subunit (Crawley et al. 2016) (data not shown). Although we cannot rule out that SMC-1::GFP spots were too small to be detected, this suggests that cohesin is not involved in the formation of the loop compartment. In another study, a clique of strong enhancers referred to as “super-enhancers” was shown to create a similar dotted line of cohesin-independent loops on HiC maps in mammalian cells (Rao et al. 2017). These contacts even included contacts between loci located on different chromosomes. Despite the striking similarity between HiC maps, we did not observe such *trans* contacts, nor any correlation with putative worm super-enhancers (Chen et al. 2020). Together, this suggests that factors other than cohesin or enhancer bound proteins are involved in loop anchor clustering.

We next wondered whether these condensin I/I^{DC}-independent loop anchors would cluster together in pairs or whether more than two anchors would come together. We therefore examined HiC reads with three or more loci ligated together (726’736 and 635’546 3-way contacts on the X chromosome for TEV control and condensin I/I^{DC} cleavage, respectively) and constructed three-dimensional contact maps at lower resolution (50 kb, Fig. 3H) (Rao et al. 2017; Rowley et al. 2020; Allahyar et al. 2018). Using those maps, we analyzed whether loop anchors form clusters, comparing all combinations of three anchors with more than 500 kb between them, as well as combinations between a control set of loci located 500 kb away from the anchors (Fig. 3H). We detected 3-way contacts between loop anchors in the TEV control situation, confirming the fact that *rex* sites in loop anchors cluster together (Rowley et al. 2020). Upon condensin I/I^{DC} cleavage, 3-way contact frequency between loop anchors increased more than two-fold demonstrating that at least three loop anchors come together. No significant 3-way contacts were observed for control loci in TEV control and upon condensin I/I^{DC} cleavage. These findings indicate that condensin I/I^{DC}-independent loop anchors tend to form clusters involving three or more loci, suggesting a rosette-like structure of the X chromosome, where anchors assemble in one or more central hubs to which individual TADs are attached.

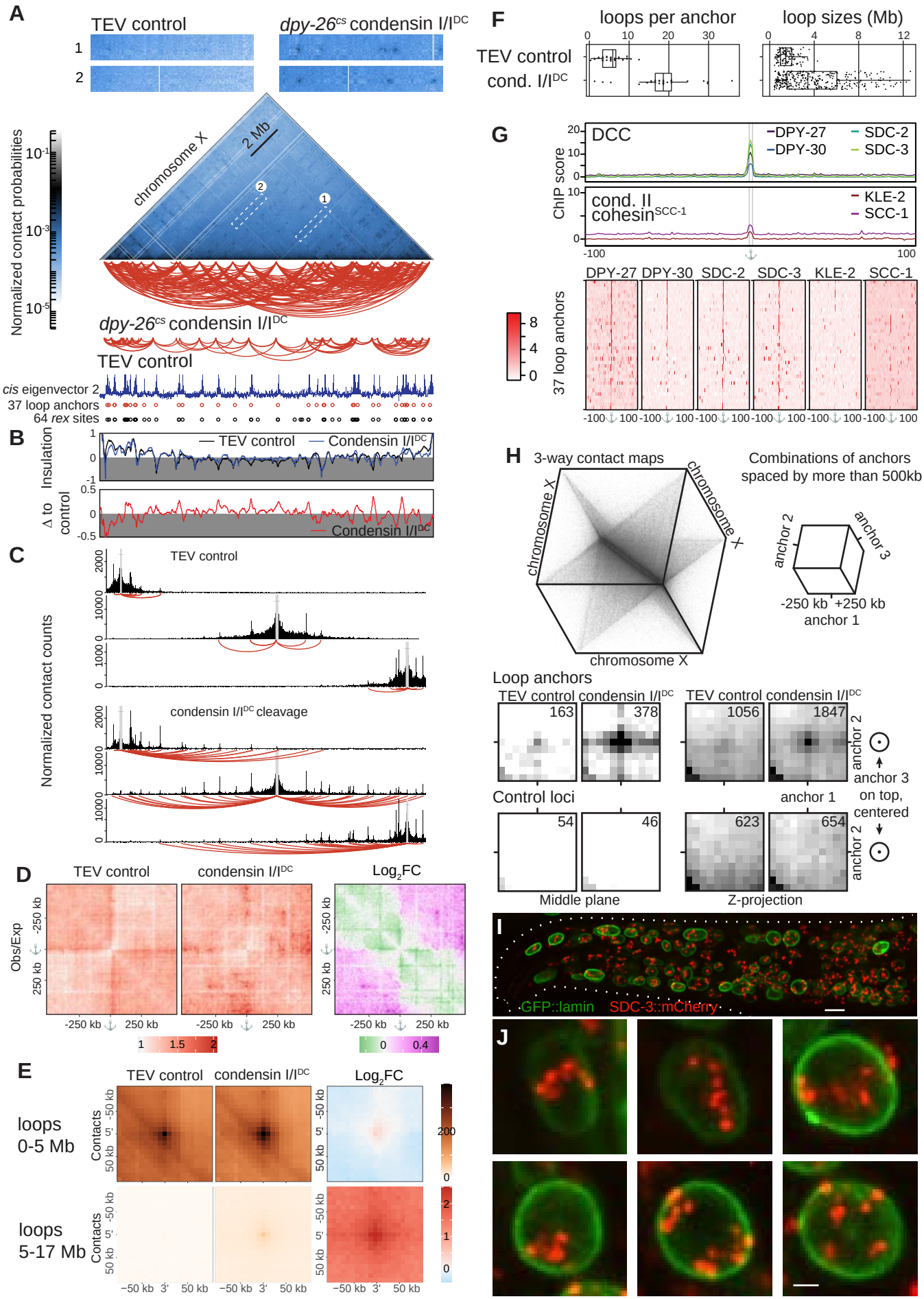
A
TEV control
dpy-26cs condensin I/IDC
chromosome X
2 Mb
Normalized contact probabilities
dpy-26cs condensin I/IDC
TEV control
cis eigenvector 2
37 loop anchors
64 rex sites
B
Insulation
Δ to control
TEV control
Condensin I/IDC
C
TEV control
condensin I/IDC cleavage
Normalized contact counts
D
TEV control
condensin I/IDC
Log2FC
Obs/Exp
-250 kb
250 kb
E
loops 0-5 Mb
loops 5-17 Mb
Contacts
F
loops per anchor
loop sizes (Mb)
TEV control
cond. I/IDC
G
DCC
DPY-27
DPY-30
SDC-2
SDC-3
cond. II cohesinSCC-1
KLE-2
SCC-1
ChIP score
37 loop anchors
H
3-way contact maps
chromosome X
Combinations of anchors spaced by more than 500kb
anchor 1
anchor 2
anchor 3
-250 kb
+250 kb
Loop anchors
Control loci
Middle plane
Z-projection
I
GFP::lamin
SDC-3::mCherry
J

Figure 3 – The hermaphrodite X chromosomes form a rosette-like structure. A. Top: comparison of regions depicted in the X chromosome HiC map highlighting the formation of dotted lines of high contact probability. Bottom: HiC contact frequency matrices upon cleavage of condensin I/I^{DC}. Lower tracks: chromatin loops depicted as arches for each condition, second *cis* eigenvector for condensin I/I^{DC}, used for loop anchor detection (local maxima), corresponding loop anchors and *rex* sites (Albritton et al. 2017). **B.** Insulation scores for matrices in 2B and the difference between them. **C.** Virtual 4C analysis on 3 representative loop anchors in the TEV control and upon condensin I/I^{DC} cleavage. **D.** Aggregated Region Analysis (ARA) on the anchors defined upon condensin I/I^{DC} cleavage, highlighting their function as boundaries in the TEV control experiment and their disappearance upon condensin I/I^{DC} cleavage. **E.** Aggregated Peak Analysis (APA) of all short (<5Mb) and long range loops (>5Mb) in TEV control and upon condensin I/I^{DC} cleavage. **F.** Number of loops per anchor and loop sizes for the two conditions in 2B. **G.** Average (top) and individual (bottom) ChIP-seq enrichment of the protein subunits of DCC (DPY-27 - L3 animals, DPY-30, SDC-2, SDC-3 - embryos), condensin II (KLE-2 - L3 animals) and cohesin (SCC-1 - L3 animals) for the 37 loop anchors detected upon condensin I/I^{DC} cleavage. Data from Kranz et al. (2013), Kramer et al. (2015), (Albritton et al. 2017) and (Huang et al. 2021). **H.** Detection of 3-way contacts between loop anchors identified in A. 3-way contact maps (top left) were built from HiC reads containing more than two fragments ligated together. Aggregated contacts between all combinations of bins containing loop anchors spaced by at least 500 kb are shown at the bottom, either the middle plane (left) or the sum Z-projection (right), in the TEV control experiment and upon condensin I/I^{DC} cleavage. The number on the upper right corner is the number of identified 3-way contacts in the middle voxel/pixel. **I.** Nuclear pattern of SDC-3::mCherry (red) in animals in control conditions expressing GFP-lamin. Bar: 5 µm. **J.** Detail of individual nuclei from the animal in I. Bar 1 µm.

The condensin I^{DC} loader complex protein SDC-3 forms nuclear clusters

Loop anchors are highly enriched for the SDC complex (Fig. 3G), and the latter is absolutely required for the enrichment of condensin I^{DC} onto the X chromosomes (Pferdehirt, Kruesi, and Meyer 2011). We therefore asked whether loop anchors would be visible *in vivo* by fluorescently labelling the SDC-3 protein at its endogenous gene location. As expected from previous studies (Davis and Meyer 1997; Yonker and Meyer 2003; Ercan et al. 2007), the protein is expressed exclusively in hermaphrodite animals, shows diffuse localization in the germline and during early embryonic development (less than 40 cells), and labels one or two nuclear territories in animals after dosage compensation onset (data not shown and Fig. 3IJ). Strikingly, SDC-3 fluorescence did not label a homogeneous chromosome territory but the protein clustered in individual spots. Little to no background fluorescence was visible outside of the clusters (Fig. 3IJ). Although linking ChIP, HiC and microscopy data is challenging (Fudenberg and Imakaev 2017), this strongly hints at the presence of loop anchor aggregates in the wild-type condition. Upon condensin I/I^{DC} cleavage, the fluorescence pattern was indistinguishable from the one observed in control animals (Fig. S5). On the one hand, this demonstrates that condensin I/I^{DC} integrity is not required for SDC-3 binding to the X chromosomes, nor for the maintenance of SDC-3 clusters. On the other hand, assuming these spots represent clustered loop anchors, the absence of modification of the fluorescence pattern strongly suggests that the rosette structure of the X chromosome is present in the control situation, yet it is not visible in HiC maps due to the high number of contacts present inside the TADs. Together, this would suggest a model for TAD formation on the X chromosome in which loop anchors are either clustered together by the activity of condensin I/I^{DC} and/or a condensin I/I^{DC}-independent mechanism involving SDC-dependent clustering of loop anchors. Anchor loci bound by the SDC complex are necessary and sufficient for the recruitment of condensin I^{DC} (Jimenez et al. 2021; Pferdehirt, Kruesi, and Meyer 2011). Recruited condensin I^{DC} would then start extruding chromatin loops asymmetrically (Ganji et al. 2018; Kong et al. 2020; Rowley et al. 2020). Loop anchors show the same very high enrichment for the DPY-27 SMC subunit of condensin I^{DC}, as the SDC subunits (Fig. 3G), suggesting that the DPY-27 part of condensin I^{DC} remains immobile, bound to the anchor locus while the other SMC globular domain (of MIX-1) progresses towards the next loop anchor, creating the TAD structure. Extrusion stops when the moving foot of the condensin reaches another loop anchor locus which plays the role of a loop extrusion barrier. Additional compaction is carried out by the random loading and extrusion by condensin I, equally present on the X chromosome and on autosomes (Kranz et al. 2013).

SDC-3 knock-down decreases TAD structure but does not increase the loop anchor compartment

SDC-3 is highly enriched at loop anchors and TAD boundaries, forms microscopically visible intranuclear clusters and is absolutely necessary for condensin I^{DC} enrichment on the X chromosomes. We therefore asked whether removing the protein would modify X chromosome structure, by tagging the protein with an auxin-inducible degron, which for a fluorescently labelled SDC-3 led to a marked decrease, yet not the complete disappearance of the fluorescence signal when animals are grown on auxin-containing medium (Fig. S10). HiC analysis showed that SDC-3 knock-down led to a decrease of the TAD structure of the X chromosomes, albeit to a lesser degree than condensin I/I^{DC} cleavage (Fig. 4A-C). This demonstrates again the dynamic nature of the TAD structures, which require the presence of SDC-3 and continuous condensin I^{DC} recruitment by the SDC complex to be maintained. In contrast to condensin I/I^{DC} cleavage, the reciprocal loop compartment did not form and contacts at loops were similar between the TEV control and upon SDC-3 knock-down (Fig. 4D). SDC-3 appears thereby to be necessary for TAD formation but not for loop maintenance, suggesting another component of the DCC leads to the formation of the clusters observed with fluorescent SDC-3 (Fig. 3IJ).

Cohesin^{SCC-1} and condensin II cleavage lead to correlated transcriptional changes

We next examined how SMC cleavage impacts on gene expression, comparing animals after cleavage to TEV control ones. With the exception of X-linked genes after cleavage of condensin I/I^{DC}, SMC cleavage led to overall modest changes in gene expression (the majority of significantly changing genes having a log2 fold change (LFC) between 0.15 and 0.5, Fig. S6A, Supplementary File 1). Exon-Intron split analysis confirmed that most changes occurred at the transcriptional level (Fig. S8) (Gaidatzis et al. 2015). Considering genes as significantly differentially expressed when |LFC|>0.5 with an adjusted p-value of 0.05, only 3-12% of genes show different expression levels (154 to 1509 genes, Fig. 5A). Upon cleavage of condensin II, cohesin^{COH-1}, cohesin^{SCC-1} or cohesin$^{COH-1/SCC-1}$, these genes were distributed evenly across all chromosomes and slightly more genes were upregulated than downregulated, suggesting a rather repressive function for SMC complexes in gene regulation (Fig. 5A, S6C). Cleavage of both cohesin^{SCC-1} and cohesin^{COH-1} kleisins led to a synergistic effect, with the highest number of misregulated genes (Fig. 5A, S6C). We observed little overlap between differentially regulated genes upon individual cleavage of the two cohesin isoforms, and the correlation of their LFC was weak (Pearson's r=0.12, Fig. 5CDE), suggesting that the two cohesin complexes have different functions or targets in gene regulation. In contrast, there was a clear correlation between differentially regulated genes upon cleavage of cohesin^{SCC-1} and condensin II (266 genes overlap, Pearson's r=0.8, Fig. 5BDE, S7AB). Gene Ontology analysis revealed a significant proportion of the genes were linked to proteolysis or stress response, possibly in relation with the shared mitotic functions of cohesin^{SCC-1} and condensin II (Supplementary File 2). This stress response was not the result of the heat shock treatment used to activate the TEV protease, as an independent dataset of genes misregulated in *kle-2* null animals (Kranz et al. 2013) similarly correlated well with our condensin II or cohesin^{SCC-1} cleavage datasets (Pearson correlation 0.22, 0.25 respectively *vs* 0.05 and 0.001 for condensin I/I^{DC} and cohesin^{COH-1}, data not shown). In summary, cleavage of either cohesins or condensin II has few transcriptional consequences, yet a common set of genes appear to be regulated by cohesin^{SCC-1} and condensin II.

Das et al., Figure 4

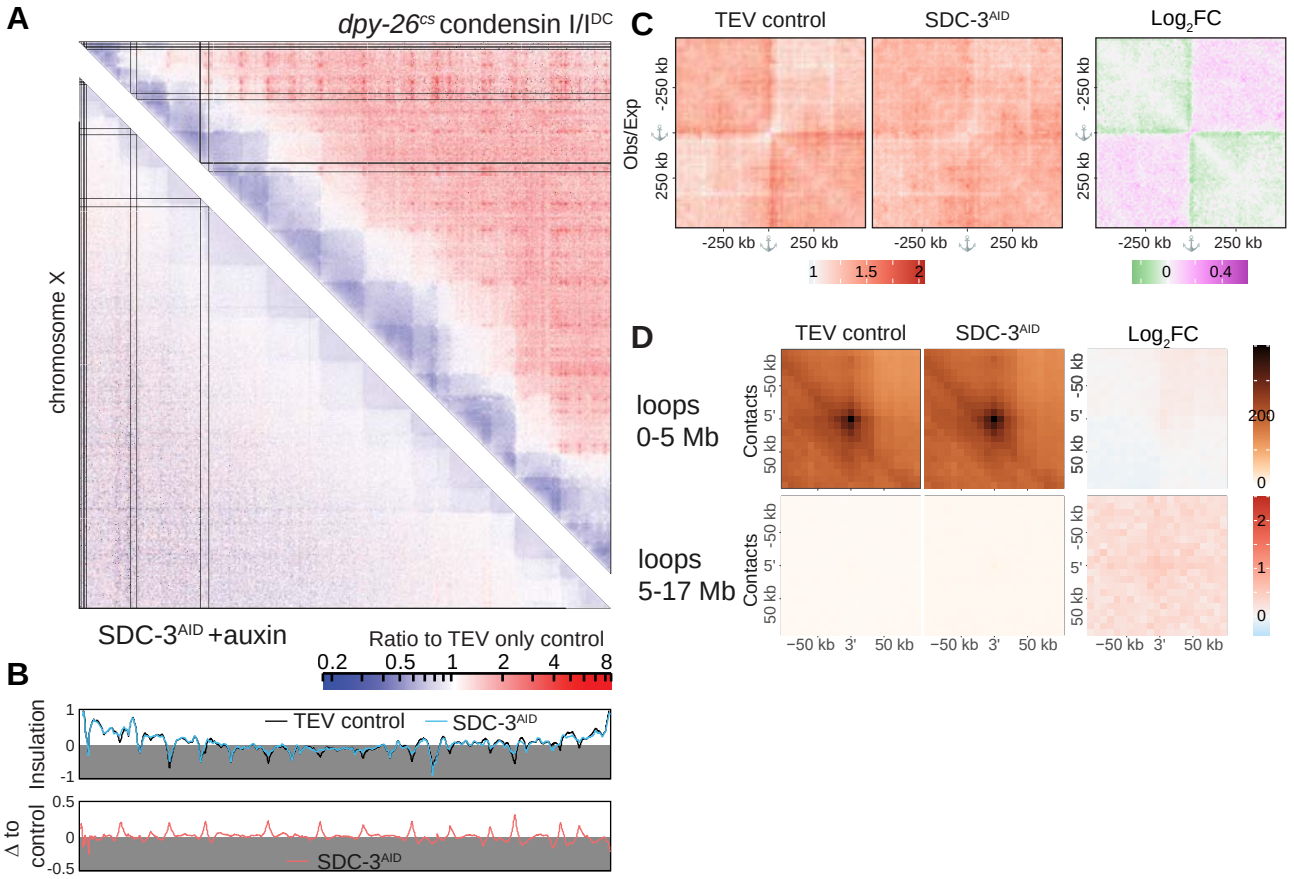

Figure 4 - Knock-down of the condensin I^{DC} loading complex protein SDC-3 down affects TAD structure, X-linked gene expression but not the X loop compartment.
A. HiC contact frequency ratio to TEV control after condensin I/I^{DC} cleavage (top right) and SDC-3 knock-down (bottom left) for the X chromosome. Pooled data from two biological replicates per condition. **B.** Insulation score for the matrix in A and difference between SDC-3 knock-down (SDC-3^{AID}) and control. **C.** ARA analysis on the anchors defined upon condensin I/I^{DC} cleavage highlighting decreased TAD organization upon SDC-3 knock-down. **D.** APA for reciprocal loops between anchors as in Fig. 3E. Loops are split by size between 0-5 Mb and >5 Mb.

Cleavage of condensin I/I^{DC} or knock-down of the X-targeting condensin I^{DC} complex mainly impacts genes on the X chromosome

Condensin I/I^{DC} cleavage led to the biggest change in gene expression on chromosome X: half of the expressed X-linked genes showed significantly higher expression (834 out of 1604), while only 4 were downregulated (52% and 0.0025% of expressed X-linked genes, respectively, Fig. 5A, S6BC). In contrast, 366 and 146 autosomal genes were up and down regulated, respectively (3.6% and 1.5% of expressed genes). The major effect of condensin I/I^{DC} cleavage on gene expression is therefore the relief of repression of X-linked genes, a consequence of the cleavage of condensin I^{DC} exclusively bound to the X chromosome (Meyer 2022). Comparison with previous datasets highlighted a significant overlap between X-linked genes upregulated by condensin I/I^{DC} cleavage, and upregulated following condensin I^{DC} RNAi knock-down or mutation of the DCC-associated DPY-21 H4K20 demethylase (25% and 46%, respectively, Fig. S11D) (Kramer et al. 2015; Brejc et al. 2017). A smaller number of genes overlapped with those regulated by $cohesin^{SCC-1}$ or condensin II cleavage (Fig. 5B, S7A), yet their gene expression change correlated only moderately even when looking only at autosomal genes (Pearson's r=0.43 and 0.29, respectively, Fig. S7B). Unlike mammalian cells upon cohesin depletion, we found no evidence for pervasive upregulation of non-coding RNAs, nor for general misregulation of transposons or repetitive sequences for $cohesin^{SCC-1}$, condensin II or condensin I/I^{DC} cleavage (data now shown and Schwarzer et al. 2017). The same result was obtained when sequencing ribosomal-depleted total RNA instead of poly-adenylated transcripts.

Interestingly, X-linked gene upregulation in close vicinity to the loop anchors characterized above and bound by the SDC complex was significantly lower upon condensin I/I^{DC} cleavage (Fig. 5F, S7C). In non-anchor regions, 48% of genes (823 of 1707) were significantly upregulated, while in 10 kilobases regions around loop anchors, only 11% of genes (6 of 55) were upregulated, indicating that gene regulation is largely maintained close to sites bound by the SDC subunits of the DCC.

In contrast to previous experiments, our experimental approach is based on the release of condensin I/I^{DC} from chromatin, rather than the analysis of genetic mutants for which dosage compensation cannot be established. The X-specific increase in gene expression thereby demonstrates that condensin I/I^{DC} ongoing presence on chromatin is essential to maintain X-linked gene regulation, and not the consequence of secondary chromatin modifications which in turn regulate gene expression independently of condensin I^{DC}. As condensins have been shown to be able to extrude both DNA and chromatin loops *in vitro* (Ganji et al. 2018; Kong et al. 2020), these results, together with a recent analysis showing that the ATPase activity of DPY-27 is necessary for its binding to the X chromosome (Breimann et al. 2021) strongly suggest that condensin I^{DC} constantly extrudes loops to regulate gene expression.

Das et al., Figure 5

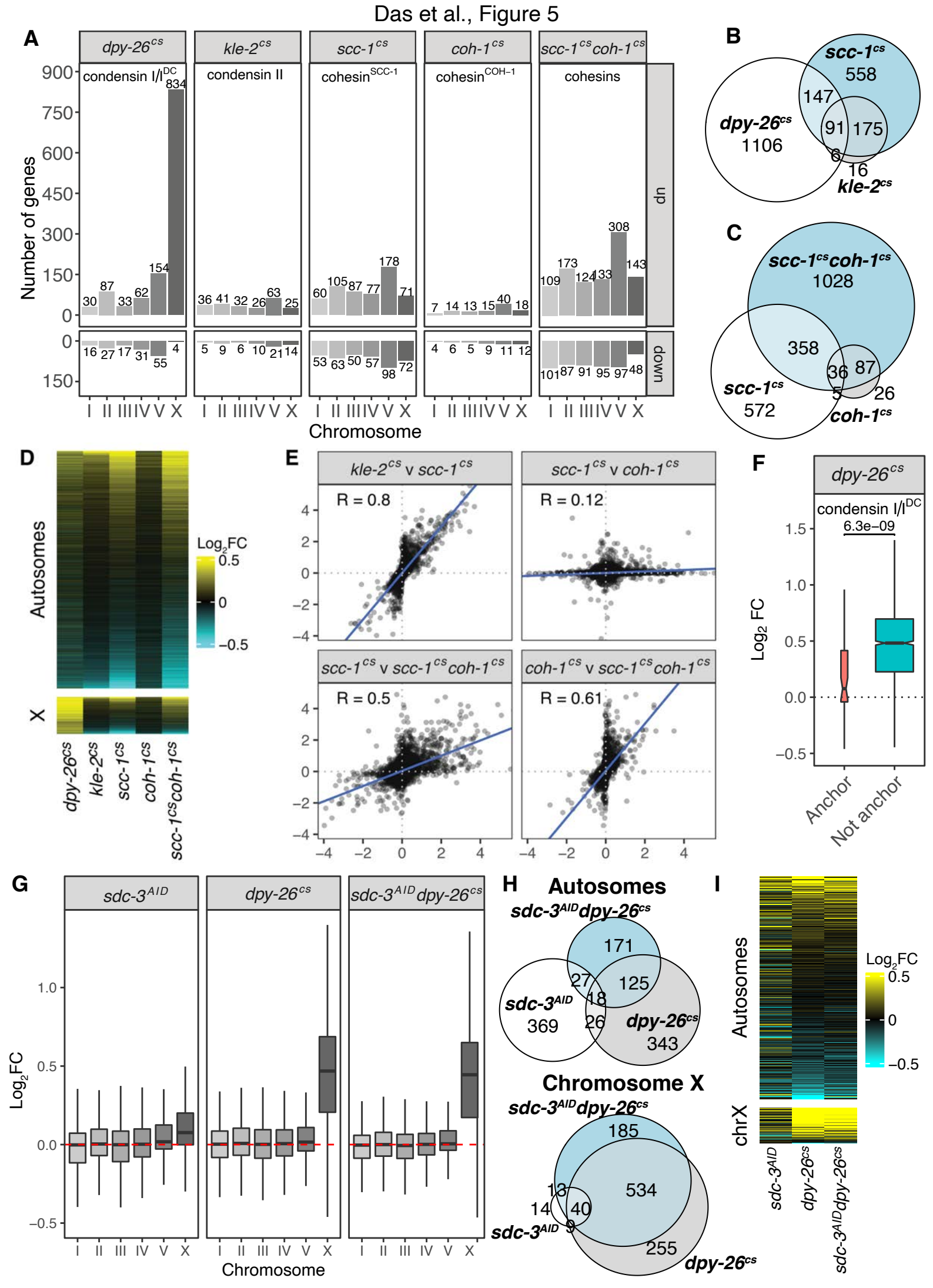

Figure 5 - Differential gene expression after cleavage of kleisin subunits of different SMC complexes. A. Number of significantly up and down regulated genes (AdjP<0.05, |LFC|>0.5) per chromosome upon cleavage of condensin I/I^{DC} (*dpy-26^{cs}*), condensin II (*kle-2^{cs}*), or the alternative kleisin subunits of cohesin, *scc-1^{cs}* and *coh-1^{cs}* individually or together. The number of up/down regulated genes is shown next to each bar. **B.** Overlap between the significantly changed genes in the condensin I/IDC, condensin II and cohesin^{SCC-1} datasets, showing a particularly strong overlap for genes misregulated by cleavage of condensin II and cohesin^{SCC-1}. **C.** Overlap between the significantly changed genes upon cleavage of cohesin^{SCC-1}, cohesin^{COH-1} or both, showing a relatively small overlap of genes misregulated by cleavage of cohesin^{SCC-1} and cohesin^{COH-1}. **D.** Hierarchical clustering of the LFC of 12465 genes filtered by DESeq2 as expressed in at least one dataset. Top panel: 10792 autosomal genes. Bottom panel: 1673 X-linked genes. **E.** Correlation of the LFC of 13734 expressed genes (with at least 10 read counts in total) from the condensin II and cohesin datasets. The blue line indicates the best fit linear regression, and the Pearson correlation coefficient is shown in each panel. **F.** Log2 fold change of expression after cleavage of condensin I/I^{DC} of 55 genes that lie in 10kb regions around 37 loop anchors defined in Fig. 3A ("Anchor"), compared with 1707 genes found on the X chromosome that do not overlap with loop anchor regions ("Not anchor"). The p-value from the Wilcoxon rank sum test comparing genes in anchor to non-anchor is shown in the panel. **G.** Log2 fold change of genes by chromosome upon SDC-3 knock-down (*sdc-3^{AID}*), condensin I/I^{DC} cleavage (*dpy-26^{cs}*) or both. **H.** Hierarchical clustering of the LFC of 11701 genes filtered by DESeq2 as expressed in at least one dataset. Top panel: 10097 autosomal genes. Bottom panel: 1604 X-linked genes. **I.** Overlap between the significantly changed genes (AdjP<0.05, |LFC|>0.5) in the *dpy-26^{cs}*, *sdc-3^{AID}* and *sdc-3^{AID}dpy-26^{cs}* datasets showing significant overlap in X-linked, but not autosomal misregulated genes. The data for *dpy-26^{cs}* in A-F is the same as that in G-I, it is included twice for the sake of comparisons.

We next analyzed the transcriptional consequences of SDC-3 auxin-mediated knockdown. In contrast to condensin I^{DC} cleavage, we observed only low to moderately higher X-linked gene expression levels (LFC 0.12 for X *vs* 0.02 for autosomes, Fig. 5G, S11AB, Supplementary File 1). Out of the 76 X-linked genes that changed upon SDC-3 degradation, 49 overlapped with genes upregulated by condensin I/I^{DC} cleavage, compared to only 44 of the 444 autosomal genes (Fig. 5H). As we compared the same strain with or without auxin, the much weaker effect of SDC-3 knock-down might be due to leaky degradation in the absence of auxin or only partial degradation of SDC-3 in the presence of auxin (Hills-Muckey et al. 2021). Alternatively, it might reflect the fact that once recruited to the X chromosomes, condensin I^{DC} does not require SDC-3 any more and is sufficient for gene regulation. Simultaneous degradation of SDC-3 and condensin I/I^{DC} cleavage resulted in a very similar transcriptional output to condensin I/I^{DC} cleavage alone, with most genes on the X chromosome upregulated (772 *vs* 834 for condensin I/I^{DC} cleavage alone, Fig. S11A) and slightly weaker average LFC (0.5 vs 0.53, Fig. 5HI).

Recent work suggests that transcription-induced supercoiling of DNA upon depletion of topoisomerase I leads to accumulation of condensin I^{DC} in gene bodies, and that this effect increases with gene length (Morao et al. 2021). We analyzed whether cleavage of the different SMCs differentially affected genes of different lengths, by comparing the LFC as a function of gene expression in the TEV control strain and gene length (Fig. S9A). If long genes accumulate more supercoiling and condensin I^{DC} one might expect that cleavage of condensin I^{DC} would alleviate this topological constraint and cause gene expression up regulation rather than down regulation. However, we saw that the longest significantly changed genes upon cleavage of condensin I/I^{DC}, condensin II and cohesin^{SCC-1} were more often down-regulated than up-regulated (Fig. S9AB). Interestingly, upon cleavage of cohesin^{COH-1} and the double cohesin$^{SCC-1/COH-1}$, the trend was the opposite: longer genes were more often upregulated (Fig. S9AB), further reinforcing the observation that cohesin^{SCC-1} and cohesin^{COH-1} complexes have different roles. Furthermore, despite cleavage of cohesin^{COH-1} having relatively small effects on transcription on its own, when both cohesin^{COH-1} and cohesin^{SCC-1} are cleaved the effects are much more similar to those of cohesin^{COH-1} cleavage alone (Fig. S7B, S9B).

Lack of dosage compensation, not autosomal chromatin decompaction, leads to reduced lifespan

Our HiC and RNA-seq data demonstrated two outcomes of condensin I/I^{DC} cleavage: genome-wide loss of chromosome compaction on both autosomes and the X chromosome, and mainly

X-specific gene upregulation due to loss of dosage compensation. Either phenomenon could cause the lifespan reduction observed upon condensin I/I^{DC} cleavage (Fig. 1D). To discriminate between these two models, we analyzed the lifespan of SDC-3^{AID} animals with and without auxin, as SDC-3 only impacts condensin I^{DC} and not condensin I (Meyer 2022). On its own, the degron tag and the auxin-binding receptor TIR1 expression had no effect on lifespan, as animals grown on media without auxin lived almost as long as TEV control animals, the slightly longer lifespan of the latter likely due to the heat-shock used to induce TEV expression (Lithgow et al. 1995). In contrast and despite the low transcriptional upregulation of X-linked genes which we observed after 22 hours on auxin, lifespan analysis - for which animals are grown on auxin for long periods of time - showed that upon SDC-3 degradation, most animals were dead by day 15 and only 4% of the animals remained alive by day 20, very similar to condensin I/I^{DC} cleavage (Fig. 1E). We conclude that lifespan reduction after condensin I/I^{DC} cleavage is not a consequence of genome-wide unfolding but due to the X-specific disruption of chromosome structure and the ensuing upregulation of X-linked genes. While our experimental system cannot discriminate between the effects of X chromosome structural changes and the transcriptional impact of these, a previous study has reported that loss of TAD structure by the deletion of a subset of the loop anchors identified above leads to a limited (17%) reduction in the mean lifespan of the animals. This is not accompanied by significant transcriptional changes in embryos, yet no transcription data was reported in older animals (Erika C. Anderson et al. 2019).

In summary, our study provides evidence for the functional replacement of cohesin by condensin I in holocentric nematodes for interphase genome folding. The impact of condensin I removal in nematodes is similar to cohesin removal in mammals, including TAD disappearance and an increase of epigenomic compartmentation. In addition, clustering of TAD boundaries on the X chromosome is highly reminiscent of super-enhancers clustering upon degradation of cohesin, highlighting a previously unknown clustering propensity of these sites in the absence of the putative chromatin loop extruder. As for mammals, SMC removal has little transcriptional output, except for the X chromosome. Loss of dosage compensation upon condensin I/I^{DC} cleavage is the main transcriptional effect and a major burden for the organism as it drastically reduces their lifespan. Studies of additional species will elucidate whether genome folding by condensin I is a peculiarity of this nematode or whether convergent evolution led to similar mechanisms in the numerous characterized other holocentric organisms (Melters et al. 2012).

Acknowledgements

We would like to thank Cihan Elcin and Michael Berger for technical help, Dr. Luca Giorgetti, Pr. Susan Gasser, Pr. Jeroen de Ridder, Dr. Amin Allahyar and Dr. Adriana Gonzalez for discussions and optimizations of the project, Dr. Pamela Nicholson and her team at the NGS platform of the University of Bern, the Meister laboratory for discussion, Dr. Kobus von Unen and the Pertz laboratory for help with microscopy. This work was funded by the Swiss National Science Foundation 31003A_176226/PP00P3_159320, the University of Bern, the SBFI ESKAS Program 2020.0321 and the Novartis Foundation for Medical/Biological Research.

Methods

Creation of TEV cleavage sites in individual kleisins and degron tagging of SDC-3

TEV cleavage sites were integrated into kleisin subunits of the different SMC complexes using CRISPR/Cas9 genome engineering (Paix et al. 2014), using *unc-58* or *dpy-10* co-CRISPR as marker. Similarly, *sdc-3* was modified N-terminally by integrating the degron sequence in frame with the protein in the HW2079 strain (kindly provided by Dr. Helge Grosshans)

expressing the TIR1 ubiquitin ligase under the control of the *eft-3* promoter. Template primers and guide RNAs are described in Supplementary Table S1.

Phenotypic characterization

Animals synchronized at the first larval stage were grown at 22°C on fresh NGM plates seeded with OP50 bacteria. After 3 hours, the animals were heat-shocked at 34°C for 30 minutes and incubated at 22°C for the rest of the experiment, while they were imaged and their phenotype quantified.

Quantification of seam cell divisions

To evaluate the progression of seam cell division, strains with TEV sites in kleisins expressing a fluorescent seam cell marker (wls[scm::gfp] V) were treated as above and the number of seam cells per animal (n = 10) was counted every 24 hours for the next three days.

RNA-seq

For strains PMW366, PMW382, PMW775, PMW784, PMW828 and PMW844 synchronized L1 nematodes were seeded on NGM plates and incubated for 3 hours at 22°C. The animals were heat-shocked at 34°C for 30 minutes to activate the TEV protease and incubated again for 19 hours at 22℃. For strains PMW821, PMW823, PMW822, synchronized L1 nematodes were seeded on NGM plates with 1 mM auxin (prepared in ethanol). As a control, the strain PMW822 was seeded on NGM plates without auxin but with ethanol. L1 worms were incubated for 3 hours at 22°C, heat-shocked at 34°C for 30 minutes and incubated for another 19 hours at 22°C. At that stage, most of the population reached the third larval stage. Animals were washed thrice with M9 buffer. RNA was isolated from the worms using Trizol, treated with DNase and cleaned using RNeasy MinElute Cleanup Kit. Sequencing libraries were created using the Illumina Stranded mRNA preparation kit. Libraries were sequenced on an Illumina Novaseq 6000 device at the NGS platform of the University of Bern.

RNA-seq data analysis

Between 37 and 60 million reads were generated from each library divided between two lanes of an Illumina NovaSeq 6000 machine. Adaptors were trimmed with Cutadapt v2.5, and reads were aligned to the WS275 version of the C. elegans protein coding transcriptome using Salmon v1.5.2 in quant mode using –seqBias –gcBias and --numBootstraps 100 options. Differential expression analysis was carried out with DESeq2 v1.34. First, all genes with less than 10 reads in total among all samples were removed. The cleavage of each of the kleisin subunit was contrasted with the control strain expressing only the TEV protease, while accounting in the design formula for variation arising from sequencing lane, biological replicate and sequencing date. Log2 fold change estimates were shrunken with the “apeglm” algorithm. An initial check showed that 35.1%, 51.5% and 49.6% of the significantly changing genes upon cleavage of DPY-26, KLE-2 and SCC-1, respectively, were genes that oscillate during larval development (Latorre et al. 2015; Meeuse et al. 2020). Oscillating genes could produce a large fold change in expression due to very small developmental asynchronies, therefore we filtered out a combined list of 4522 genes that oscillate during larval development from the DEseq2 object before analysis. Basic processing of the RNAseq data and exploratory data analysis were carried out with custom scripts in bash and R, that can be found on github (https://github.com/CellFateNucOrg/SMC_RNAseq/tree/v0.2). The scripts used to generate the figures in this paper can be found at (https://github.com/CellFateNucOrg/MoushumiDas_paper/tree/v0.2). Significantly misregulated genes were filtered with an adjusted p-value of <0.05, and we considered either all statistically significant genes, or those that also had an absolute log2 fold change >0.5, as

indicated in the figure legends. This threshold was chosen empirically to maximize the number of significant X-linked genes upon cleavage of DPY-26 while minimizing the number of autosomal genes that were considered significant.

RNAseq was performed in strains containing SDC-3 tagged with the auxin inducible degron (AID) tag and TIR1 ubiquitin ligase with and without auxin as described in Supplementary Table S5. For better comparison to previous samples, all strains contained the heat-shock inducible TEV protease and were heat shocked at the L1 stage. Mapping and differential gene expression analysis was performed with Salmon and DESeq2 as described above. DESeq2 analysis was carried out by creating a dummy variable containing all combinations of *dpy-26*^{cs}, *sdc-3*^{AID}, TIR1, and auxin treatment that were present in the data and initially all strains were compared to the PMW366 control strain without auxin, taking into account sequencing lane, biological replicate and sequencing date as control variables. More complex comparisons were carried out in DESeq2 to remove background effects of auxin and TIR1 by subtracting the coefficients of the different levels of the dummy variable. In the results we focussed on the contrasts between PMW382 and PMW366 without auxin for *dpy-26*^{cs} effects, and on the PMW822 strain with and without auxin for SDC-3 degron effects. The effect of the double mutant with both degradation of SDC-3 and cleavage of DPY-26 was estimated by subtracting the dummy variable coefficients for strain PMW823 with auxin from those of PMW821 with auxin in order to remove any non specific effects of TIR1 and auxin in the absence of the degron.

Lifespan assay

Animals were synchronized at the L1 stage and heat-shocked as above. When they reached the L4 stage, they were transferred to tight-fitting plates (BD Falcon Petri Dishes, 50x9mm) containing 50 µg/ml FUdR and permanently shifted to 20°C. For degron-mediated degradation of SDC-3, *sdc-3*^{degron}, half of the animals were transferred to FUdR plates with 1mM auxin diluted in DMSO, while the other half was transferred to FUdR plates with DMSO as a control. Plates were then loaded into air-cooled Epson V800 scanners and imaged with a frequency of two scans per hour using the lifespan machine setup (Stroustrup et al. 2013). The temperature of the scanner flatbed was continuously monitored (Thermoworks, Utah, US). Animals that exploded, burrowed or escaped the imaging area were censored. For data processing, L4 stage animals were defined as day 0 of adulthood. The Kaplan-Meier product-limit procedure followed by the null hypothesis test employing the Mantel-Cox log-rank approach was applied to derive the survival function estimates. The survival data was processed in R using packages survminer (v0.3.1) and survival (v3.1-12).

Construction of HiC libraries

3D chromatin conformation was acquired as in (Jimenez et al. 2021), using synchronized animals 19 hours after heat-shock for TEV induction as described above and with the following modifications. Animals were pelleted and stored at -80°C. For fixation, the frozen worm pellet was resuspended in 2% formaldehyde prepared in M9 buffer and incubated for 30 mins in the rotator. Formaldehyde was then quenched with glycine at 125 mM (final), incubated 5 minutes. The worms were pelleted again, washed with M9 and about 100 ul of the packed animals were transferred to a 1.5 ml microcentrifuge tube, washed with 1 ml 1x PBS and protease inhibitors, washed again with 1 ml 1x PBS, snap frozen in liquid nitrogen before -80°C storage. Cross-linked frozen worms were ground using a SPEX6775 freezer/mill (SPEX Europe) at 5 cycles per second for 1 minute with a total of 2 cycles. The ground worm powder was dissolved in 5 ml 1x PBS and immediately cross-linked with 500 µl TC buffer (100 mM NaCl, 1mM EDTA, 0.5 mM EGTA, 50 mM Hepes pH 8.0, 22% formaldehyde), to a final concentration of 2% formaldehyde for 20 minutes at room temperature. Cross-linking was stopped by addition of 289 ul of Stop Solution 1 (provided in the Arima HiC kit) and 5 minutes incubation at RT.

Samples were pelleted at 2000g for 15 mins at RT and resuspended in 5 ml 1x PBS before 10 aliquots were distributed into 1.5 ml microcentrifuge tubes. The amount of DNA acquired from a single aliquot was estimated and accordingly the subsequent HiC experiment was done as per the manufacturer's instructions. For library preparation, the modified protocol from Arima Genomics for the KAPA Hyper Prep Kit was used. The libraries were sequenced with Illumina sequencing to generate 100 bp paired end reads. Sequence data is presented in Supplementary table S3 and available from GEO (GSE199723).

HiC data analysis

HiC Illumina data was processed using the HiCPro pipeline (Servant et al. 2015). A Singularity container containing version 3.0.0 of HiCPro was run with custom bash scripts with default parameters in the config file except for customisation to the local cluster environment and the following parameters: BIN_SIZE = 2000, LIGATION_SITE = GATCGATC, GANTGATC, GANTANTC, GATCANTC for samples prepared with the Arima HiC kit, and using the ce11 genome downloaded from UCSC. The HiC-Pro results matrix was converted to cool format using the hicpro2higlass.sh tool from the Hic-Pro utils scripts. We then generated both balanced and unbalanced mcool files with our own custom resolutions ('2000,4000,6000,8000,10000,20000,50000,100000,200000,500000') with the cooler software (version 0.8.6) so they could be viewed in HiGlass. The custom bash scripts can be found in (https://github.com/CellFateNucOrg/hicpro/tree/v0.1). Additional data analysis was conducted with cooltools (Venev et al. 2021), GENOVA (van der Weide et al. 2021) and ad-hoc R scripts. For 3-way contacts analysis, forward and reverse reads which did not aligned in the first round of "global" alignment of HiCPro were fused together *in vitro* and processed using the MC-HiC pipeline (Allahyar et al. 2018), using a 50 kb bin size and the bowtie2 mapper with parameters --very-sensitive -L 20 --score-min L,-0.6,-0.2 --end-to-end.

References

Abdennur, N., W. Schwarzer, A. Pekowska, and I. A. Shaltiel. 2018. "Condensin II Inactivation in Interphase Does Not Affect Chromatin Folding or Gene Expression." *BioRxiv*. https://www.biorxiv.org/content/10.1101/437459v1.abstract.

Albritton, Sarah Elizabeth, Anna-Lena Kranz, Lara Heermans Winterkorn, Lena Annika Street, and Sevinc Ercan. 2017. "Cooperation between a Hierarchical Set of Recruitment Sites Targets the X Chromosome for Dosage Compensation." *eLife* 6 (May). https://doi.org/10.7554/eLife.23645.

Allahyar, Amin, Carlo Vermeulen, Britta A. M. Bouwman, Peter H. L. Krijger, Marjon J. A. M. Verstegen, Geert Geeven, Melissa van Kranenburg, et al. 2018. "Enhancer Hubs and Loop Collisions Identified from Single-Allele Topologies." *Nature Genetics* 50 (8): 1151–60.

Anderson, E. C., Q. Yang, and B. J. Meyer. 2020. "Histone H3K9 Methylation Promotes Formation of Genome Compartments in Caenorhabditis Elegans via Chromosome Compaction and Perinuclear Anchoring." *Proceedings of the*. https://www.pnas.org/content/117/21/11459.short?casa_token=eV0f0ZCBvW8AAAAA:ziwEkrwFsiwiTHGUXPOrGj0ISrV74Mh7Iu63ek1aAHGQd-7k-HC0muveEX3rC-_AbQYD2m0gsogzvmI.

Anderson, Erika C., Phillip A. Frankino, Ryo Higuchi-Sanabria, Qiming Yang, Qian Bian, Katie Podshivalova, Aram Shin, Cynthia Kenyon, Andrew Dillin, and Barbara J. Meyer. 2019. "X Chromosome Domain Architecture Regulates Caenorhabditis Elegans Lifespan but Not Dosage Compensation." *Developmental Cell* 51 (2): 192–207.e6.

Angeles-Albores, David, Raymond Lee, Juancarlos Chan, and Paul Sternberg. 2018. "Two New Functions in the WormBase Enrichment Suite." *microPublication Biology* 2018 (March). https://doi.org/10.17912/W25Q2N.

Bian, Qian, Erika C. Anderson, Qiming Yang, and Barbara J. Meyer. 2020. “Histone H3K9 Methylation Promotes Formation of Genome Compartments in *Caenorhabditis Elegans* via Chromosome Compaction and Perinuclear Anchoring.” *Proceedings of the National Academy of Sciences*. https://doi.org/10.1073/pnas.2002068117.

Breimann, Laura, Ana Karina Morao, Jun Kim, David Sebastian Jimenez, Nina Maryn, Krishna Bikkasani, Michael J. Carrozza, et al. 2021. “The H4K20 Demethylase DPY-21 Regulates the Dynamics of Condensin DC Binding.” *Journal of Cell Science*, December. https://doi.org/10.1242/jcs.258818.

Brejc, Katjuša, Qian Bian, Satoru Uzawa, Bayly S. Wheeler, Erika C. Anderson, David S. King, Philip J. Kranzusch, Christine G. Preston, and Barbara J. Meyer. 2017. “Dynamic Control of X Chromosome Conformation and Repression by a Histone H4K20 Demethylase.” *Cell* 171 (1): 85–102.e23.

Cattoni, Diego I., Andrés M. Cardozo Gizzi, Mariya Georgieva, Marco Di Stefano, Alessandro Valeri, Delphine Chamousset, Christophe Houbron, et al. 2017. “Single-Cell Absolute Contact Probability Detection Reveals Chromosomes Are Organized by Multiple Low-Frequency yet Specific Interactions.” *Nature Communications* 8 (1): 1753.

Chan, Raymond C., Annette Chan, Mili Jeon, Tammy F. Wu, Danielle Pasqualone, Ann E. Rougvie, and Barbara J. Meyer. 2003. “Chromosome Cohesion Is Regulated by a Clock Gene Paralogue TIM-1.” *Nature* 423 (6943): 1002–9.

Chen, Chuangeng, Dianshuang Zhou, Yue Gu, Cong Wang, Mengyan Zhang, Xiangyu Lin, Jie Xing, Hongli Wang, and Yan Zhang. 2020. “SEA Version 3.0: A Comprehensive Extension and Update of the Super-Enhancer Archive.” *Nucleic Acids Research* 48 (D1): D198–203.

Crane, Emily, Qian Bian, Rachel Patton McCord, Bryan R. Lajoie, Bayly S. Wheeler, Edward J. Ralston, Satoru Uzawa, Job Dekker, and Barbara J. Meyer. 2015. “Condensin-Driven Remodelling of X Chromosome Topology during Dosage Compensation.” *Nature* 523 (7559): 240–44.

Crawley, Oliver, Consuelo Barroso, Sarah Testori, Nuria Ferrandiz, Nicola Silva, Maikel Castellano-Pozo, Angel Luis Jaso-Tamame, and Enrique Martinez-Perez. 2016. “Cohesin-Interacting Protein WAPL-1 Regulates Meiotic Chromosome Structure and Cohesion by Antagonizing Specific Cohesin Complexes.” *eLife* 5 (February): e10851.

Csankovszki, G., K. Collette, K. Spahl, J. Carey, M. Snyder, E. Petty, U. Patel, et al. 2009. “Three Distinct Condensin Complexes Control C. Elegans Chromosome Dynamics.” *Current Biology: CB* 19 (1): 9–19.

Daugherty, Aaron C., Robin W. Yeo, Jason D. Buenrostro, William J. Greenleaf, Anshul Kundaje, and Anne Brunet. 2017. “Chromatin Accessibility Dynamics Reveal Novel Functional Enhancers in C. Elegans.” *Genome Research* 27 (12): 2096–2107.

Davidson, Iain F., Benedikt Bauer, Daniela Goetz, Wen Tang, Gordana Wutz, and Jan-Michael Peters. 2019. “DNA Loop Extrusion by Human Cohesin.” *Science* 366 (6471): 1338–45.

Davis, T. L., and B. J. Meyer. 1997. “SDC-3 Coordinates the Assembly of a Dosage Compensation Complex on the Nematode X Chromosome.” *Development* 124 (5): 1019–31.

Dekker, Job, Karsten Rippe, Martijn Dekker, and Nancy Kleckner. 2002. “Capturing Chromosome Conformation.” *Science* 295 (5558): 1306–11.

Dixon, Jesse R., Inkyung Jung, Siddarth Selvaraj, Yin Shen, Jessica E. Antosiewicz-Bourget, Ah Young Lee, Zhen Ye, et al. 2015. “Chromatin Architecture Reorganization during Stem Cell Differentiation.” *Nature* 518 (7539): 331–36.

Ercan, S., P. G. Giresi, C. M. Whittle, X. Zhang, R. D. Green, and J. D. Lieb. 2007. “X Chromosome Repression by Localization of the C. Elegans Dosage Compensation Machinery to Sites of Transcription Initiation.” *Nature Genetics* 39 (3): 403–8.

Evans, Kenneth J., Ni Huang, Przemyslaw Stempor, Michael A. Chesney, Thomas A. Down, and Julie Ahringer. 2016. “Stable Caenorhabditis Elegans Chromatin Domains Separate Broadly Expressed and Developmentally Regulated Genes.” *Proceedings of the National Academy of Sciences of the United States of America* 113 (45): E7020–29.

Flavahan, William A., Yotam Drier, Brian B. Liau, Shawn M. Gillespie, Andrew S. Venteicher, Anat O. Stemmer-Rachamimov, Mario L. Suvà, and Bradley E. Bernstein. 2016. “Insulator Dysfunction and Oncogene Activation in IDH Mutant Gliomas.” *Nature* 529 (7584): 110–14.

Fudenberg, Geoffrey, and Maxim Imakaev. 2017. “FISH-Ing for Captured Contacts: Towards Reconciling FISH and 3C.” *Nature Methods* 14 (7): 673–78.

Fudenberg, Geoffrey, Maxim Imakaev, Carolyn Lu, Anton Goloborodko, Nezar Abdennur, and Leonid A. Mirny. 2016. “Formation of Chromosomal Domains by Loop Extrusion.” *Cell Reports* 15 (9): 2038–49.

Gaidatzis, Dimos, Lukas Burger, Maria Florescu, and Michael B. Stadler. 2015. “Analysis of Intronic and Exonic Reads in RNA-Seq Data Characterizes Transcriptional and Post-Transcriptional Regulation.” *Nature Biotechnology* 33 (7): 722–29.

Ganji, Mahipal, Indra A. Shaltiel, Shveta Bisht, Eugene Kim, Ana Kalichava, Christian H. Haering, and Cees Dekker. 2018. “Real-Time Imaging of DNA Loop Extrusion by Condensin.” *Science*. https://doi.org/10.1126/science.aar7831.

Gerlich, Daniel, Toru Hirota, Birgit Koch, Jan-Michael Peters, and Jan Ellenberg. 2006. “Condensin I Stabilizes Chromosomes Mechanically through a Dynamic Interaction in Live Cells.” *Current Biology: CB* 16 (4): 333–44.

Golfier, Stefan, Thomas Quail, Hiroshi Kimura, and Jan Brugués. 2020. “Cohesin and Condensin Extrude DNA Loops in a Cell Cycle-Dependent Manner.” *eLife* 9 (May). https://doi.org/10.7554/eLife.53885.

Gonzalez-Aguilera, C., K. Ikegami, C. Ayuso, A. de Luis, M. Iniguez, J. Cabello, J. D. Lieb, and P. Askjaer. 2014. “Genome-Wide Analysis Links Emerin to Neuromuscular Junction Activity in Caenorhabditis Elegans.” *Genome Biology* 15 (2): R21.

Gonzalez-Sandoval, Adriana, Benjamin D. Towbin, Veronique Kalck, Daphne S. Cabianca, Dimos Gaidatzis, Michael H. Hauer, Liqing Geng, et al. 2015. “Perinuclear Anchoring of H3K9-Methylated Chromatin Stabilizes Induced Cell Fate in C. Elegans Embryos.” *Cell* 163 (6): 1333–47.

Haarhuis, Judith H. I., Robin H. van der Weide, Vincent A. Blomen, J. Omar Yáñez-Cuna, Mario Amendola, Marjon S. van Ruiten, Peter H. L. Krijger, et al. 2017. “The Cohesin Release Factor WAPL Restricts Chromatin Loop Extension.” *Cell* 169 (4): 693–707.e14.

Haering, C. H., and S. Gruber. 2016. “SnapShot: SMC Protein Complexes Part I.” *Cell* 164 (1-2): 326–326 e1.

Hagstrom, Kirsten A., Victor F. Holmes, Nicholas R. Cozzarelli, and Barbara J. Meyer. 2002. “C. Elegans Condensin Promotes Mitotic Chromosome Architecture, Centromere Organization, and Sister Chromatid Segregation during Mitosis and Meiosis.” *Genes & Development* 16 (6): 729–42.

Hills-Muckey, Kelly, Michael A. Q. Martinez, Natalia Stec, Shilpa Hebbar, Joanne Saldanha, Taylor N. Medwig-Kinney, Frances E. Q. Moore, et al. 2021. “An Engineered, Orthogonal Auxin analog/AtTIR1(F79G) Pairing Improves Both Specificity and Efficacy of the Auxin Degradation System in Caenorhabditis Elegans.” *Genetics*, October. https://doi.org/10.1093/genetics/iyab174.

Hirota, Toru, Daniel Gerlich, Birgit Koch, Jan Ellenberg, and Jan-Michael Peters. 2004. “Distinct Functions of Condensin I and II in Mitotic Chromosome Assembly.” *Journal of Cell Science* 117 (Pt 26): 6435–45.

Hnisz, Denes, Abraham S. Weintraub, Daniel S. Day, Anne-Laure Valton, Rasmus O. Bak, Charles H. Li, Johanna Goldmann, et al. 2016. “Activation of Proto-Oncogenes by Disruption of Chromosome Neighborhoods.” *Science* 351 (6280): 1454–58.

Huang, Ni, Wei Qiang Seow, Alex Appert, Yan Dong, Przemyslaw Stempor, and Julie Ahringer. 2021. “Accessible Region Conformation Capture (ARC-C) Gives High Resolution Insights into Genome Architecture and Regulation.” *Genome Research*, December. https://doi.org/10.1101/gr.275669.121.

Ikegami, K., T. A. Egelhofer, S. Strome, and J. D. Lieb. 2010. “Caenorhabditis Elegans Chromosome Arms Are Anchored to the Nuclear Membrane via Discontinuous Association with LEM-2.” *Genome Biology* 11 (12): R120.

Iwasaki, Osamu, Christopher J. Corcoran, and Ken-Ichi Noma. 2016. “Involvement of Condensin-Directed Gene Associations in the Organization and Regulation of Chromosome Territories during the Cell Cycle.” *Nucleic Acids Research* 44 (8): 3618–28.
Jänes, Jürgen, Yan Dong, Michael Schoof, Jacques Serizay, Alex Appert, Chiara Cerrato, Carson Woodbury, et al. 2018. “Chromatin Accessibility Dynamics across C. Elegans Development and Ageing.” *eLife* 7 (October). https://doi.org/10.7554/eLife.37344.
Jimenez, D. S., J. Kim, B. Ragipani, B. Zhang, and L. A. Street. 2021. “Condensin DC Spreads Linearly and Bidirectionally from Recruitment Sites to Create Loop-Anchored TADs in C. Elegans.” *bioRxiv*. https://www.biorxiv.org/content/10.1101/2021.03.23.436694v1.abstract.
Kakui, Yasutaka, Christopher Barrington, David J. Barry, Tereza Gerguri, Xiao Fu, Paul A. Bates, Bhavin S. Khatri, and Frank Uhlmann. 2020. “Fission Yeast Condensin Contributes to Interphase Chromatin Organization and Prevents Transcription-Coupled DNA Damage.” *Genome Biology* 21 (1): 272.
Kerpedjiev, Peter, Nezar Abdennur, Fritz Lekschas, Chuck McCallum, Kasper Dinkla, Hendrik Strobelt, Jacob M. Luber, et al. 2018. “HiGlass: Web-Based Visual Exploration and Analysis of Genome Interaction Maps.” *Genome Biology*. https://doi.org/10.1186/s13059-018-1486-1.
Koh, K., and J. H. Rothman. 2001. “ELT-5 and ELT-6 Are Required Continuously to Regulate Epidermal Seam Cell Differentiation and Cell Fusion in C. Elegans.” *Development* 128 (15): 2867–80.
Kong, Muwen, Erin E. Cutts, Dongqing Pan, Fabienne Beuron, Thangavelu Kaliyappan, Chaoyou Xue, Edward P. Morris, Andrea Musacchio, Alessandro Vannini, and Eric C. Greene. 2020. “Human Condensin I and II Drive Extensive ATP-Dependent Compaction of Nucleosome-Bound DNA.” *Molecular Cell* 79 (1): 99–114.e9.
Kramer, Maxwell, Anna-Lena Kranz, Amanda Su, Lara H. Winterkorn, Sarah Elizabeth Albritton, and Sevinc Ercan. 2015. “Developmental Dynamics of X-Chromosome Dosage Compensation by the DCC and H4K20me1 in C. Elegans.” *PLoS Genetics* 11 (12): e1005698.
Kranz, Anna-Lena, Chen-Yu Jiao, Lara Heermans Winterkorn, Sarah Elizabeth Albritton, Maxwell Kramer, and Sevinç Ercan. 2013. “Genome-Wide Analysis of Condensin Binding in Caenorhabditis Elegans.” *Genome Biology* 14 (10): R112.
Latorre, Isabel, Michael A. Chesney, Jacob M. Garrigues, Przemyslaw Stempor, Alex Appert, Mirko Francesconi, Susan Strome, and Julie Ahringer. 2015. “The DREAM Complex Promotes Gene Body H2A.Z for Target Repression.” *Genes & Development* 29 (5): 495–500.
Lieberman-Aiden, E., N. L. van Berkum, L. Williams, M. Imakaev, T. Ragoczy, A. Telling, I. Amit, et al. 2009. “Comprehensive Mapping of Long-Range Interactions Reveals Folding Principles of the Human Genome.” *Science* 326 (5950): 289–93.
Lithgow, G. J., T. M. White, S. Melov, and T. E. Johnson. 1995. “Thermotolerance and Extended Life-Span Conferred by Single-Gene Mutations and Induced by Thermal Stress.” *Proceedings of the National Academy of Sciences of the United States of America* 92 (16): 7540–44.
Liu, Tao, Andreas Rechtsteiner, Thea A. Egelhofer, Anne Vielle, Isabel Latorre, Ming-Sin Cheung, Sevinc Ercan, et al. 2011. “Broad Chromosomal Domains of Histone Modification Patterns in C. Elegans.” *Genome Research* 21 (2): 227–36.
Li, Yan, Judith H. I. Haarhuis, Ángela Sedeño Cacciatore, Roel Oldenkamp, Marjon S. van Ruiten, Laureen Willems, Hans Teunissen, et al. 2020. “The Structural Basis for cohesin–CTCF-Anchored Loops.” *Nature* 578 (7795): 472–76.
Lupianez, D. G., K. Kraft, V. Heinrich, P. Krawitz, F. Brancati, E. Klopocki, D. Horn, et al. 2015. “Disruptions of Topological Chromatin Domains Cause Pathogenic Rewiring of Gene-Enhancer Interactions.” *Cell* 161 (5): 1012–25.
Maddox, Paul S., Nathan Portier, Arshad Desai, and Karen Oegema. 2006. “Molecular Analysis of Mitotic Chromosome Condensation Using a Quantitative Time-Resolved

Fluorescence Microscopy Assay." *Proceedings of the National Academy of Sciences of the United States of America* 103 (41): 15097–102.
Ma, Hanhui, Janel R. McLean, Lucy Fang-I Chao, Sebastian Mana-Capelli, Murugan Paramasivam, Kirsten A. Hagstrom, Kathleen L. Gould, and Dannel McCollum. 2012. "A Highly Efficient Multifunctional Tandem Affinity Purification Approach Applicable to Diverse Organisms." *Molecular & Cellular Proteomics: MCP* 11 (8): 501–11.
Meeuse, Milou Wm, Yannick P. Hauser, Lucas J. Morales Moya, Gert-Jan Hendriks, Jan Eglinger, Guy Bogaarts, Charisios Tsiairis, and Helge Großhans. 2020. "Developmental Function and State Transitions of a Gene Expression Oscillator in Caenorhabditis Elegans." *Molecular Systems Biology* 16 (7): e9498.
Meister, Peter, Benjamin D. Towbin, Brietta L. Pike, Aaron Ponti, and Susan M. Gasser. 2010. "The Spatial Dynamics of Tissue-Specific Promoters during C. Elegans Development." *Genes & Development* 24 (8): 766–82.
Melters, Daniël P., Leocadia V. Paliulis, Ian F. Korf, and Simon W. L. Chan. 2012. "Holocentric Chromosomes: Convergent Evolution, Meiotic Adaptations, and Genomic Analysis." *Chromosome Research: An International Journal on the Molecular, Supramolecular and Evolutionary Aspects of Chromosome Biology* 20 (5): 579–93.
Meyer, Barbara J. 2022. "Mechanisms of Sex Determination and X-Chromosome Dosage Compensation." *Genetics*, January. https://doi.org/10.1093/genetics/iyab197.
Mito, Yoshiko, Asako Sugimoto, and Masayuki Yamamoto. 2003. "Distinct Developmental Function of Two Caenorhabditis Elegans Homologs of the Cohesin Subunit Scc1/Rad21." *Molecular Biology of the Cell* 14 (6): 2399–2409.
Morao, Ana Karina, Jun Kim, Daniel Obaji, Siyu Sun, and Sevinc Ercan. 2021. "Topoisomerases I and II Facilitate Condensin DC Translocation to Organize and Repress X Chromosomes in C. Elegans." *bioRxiv*. https://doi.org/10.1101/2021.11.30.470639.
Nora, Elphège P., Bryan R. Lajoie, Edda G. Schulz, Luca Giorgetti, Ikuhiro Okamoto, Nicolas Servant, Tristan Piolot, et al. 2012. "Spatial Partitioning of the Regulatory Landscape of the X-Inactivation Centre." *Nature* 485 (7398): 381–85.
Nuebler, Johannes, Geoffrey Fudenberg, Maxim Imakaev, Nezar Abdennur, and Leonid A.
Mirny. 2018. "Chromatin Organization by an Interplay of Loop Extrusion and Compartmental Segregation." *Proceedings of the National Academy of Sciences of the United States of America* 115 (29): E6697–6706.
Paix, Alexandre, Yuemeng Wang, Harold E. Smith, Chih-Yung S. Lee, Deepika Calidas, Tu Lu, Jarrett Smith, Helen Schmidt, Michael W. Krause, and Geraldine Seydoux. 2014. "Scalable and Versatile Genome Editing Using Linear DNAs with Microhomology to Cas9 Sites in Caenorhabditis Elegans." *Genetics* 198 (4): 1347–56.
Pasierbek, Pawel, Mathilde Födermayr, Verena Jantsch, Michael Jantsch, Dieter Schweizer, and Josef Loidl. 2003. "The Caenorhabditis Elegans SCC-3 Homologue Is Required for Meiotic Synapsis and for Proper Chromosome Disjunction in Mitosis and Meiosis." *Experimental Cell Research* 289 (2): 245–55.
Pferdehirt, Rebecca R., William S. Kruesi, and Barbara J. Meyer. 2011. "An MLL/COMPASS Subunit Functions in the C. Elegans Dosage Compensation Complex to Target X Chromosomes for Transcriptional Regulation of Gene Expression." *Genes & Development* 25 (5): 499–515.
Rao, Suhas S. P., Su-Chen Huang, Brian Glenn St Hilaire, Jesse M. Engreitz, Elizabeth M. Perez, Kyong-Rim Kieffer-Kwon, Adrian L. Sanborn, et al. 2017. "Cohesin Loss Eliminates All Loop Domains." *Cell* 171 (2): 305–20.e24.
Roayaei Ardakany, Abbas, Halil Tuvan Gezer, Stefano Lonardi, and Ferhat Ay. 2020. "Mustache: Multi-Scale Detection of Chromatin Loops from Hi-C and Micro-C Maps Using Scale-Space Representation." *Genome Biology* 21 (1): 256.
Rosin, Leah F., Son C. Nguyen, and Eric F. Joyce. 2018. "Condensin II Drives Large-Scale Folding and Spatial Partitioning of Interphase Chromosomes in Drosophila Nuclei." *PLoS Genetics* 14 (7): e1007393.

Rowley, M. Jordan, Axel Poulet, Michael H. Nichols, Brianna J. Bixler, Adrian L. Sanborn, Elizabeth A. Brouhard, Karen Hermetz, et al. 2020. “Analysis of Hi-C Data Using SIP Effectively Identifies Loops in Organisms from C. Elegans to Mammals.” *Genome Research* 30 (3): 447–58.

Sanborn, A. L., S. S. Rao, S. C. Huang, N. C. Durand, M. H. Huntley, A. I. Jewett, I. D. Bochkov, et al. 2015. “Chromatin Extrusion Explains Key Features of Loop and Domain Formation in Wild-Type and Engineered Genomes.” *Proceedings of the National Academy of Sciences of the United States of America*. https://doi.org/10.1073/pnas.1518552112.

Sawh, Ahilya N., Maxwell E. R. Shafer, Jun-Han Su, Xiaowei Zhuang, Siyuan Wang, and Susan E. Mango. 2020. “Lamina-Dependent Stretching and Unconventional Chromosome Compartments in Early C. Elegans Embryos.” *Molecular Cell* 78 (1): 96–111.e6.

Schwarzer, Wibke, Nezar Abdennur, Anton Goloborodko, Aleksandra Pekowska, Geoffrey Fudenberg, Yann Loe-Mie, Nuno A. Fonseca, et al. 2017. “Two Independent Modes of Chromatin Organization Revealed by Cohesin Removal.” *Nature* 551 (7678): 51–56.

Seitan, Vlad C., Peter Banks, Steve Laval, Nazia A. Majid, Dale Dorsett, Amer Rana, Jim Smith, et al. 2006. “Metazoan Scc4 Homologs Link Sister Chromatid Cohesion to Cell and Axon Migration Guidance.” *PLoS Biology* 4 (8): e242.

Servant, Nicolas, Nelle Varoquaux, Bryan R. Lajoie, Eric Viara, Chong-Jian Chen, Jean-Philippe Vert, Edith Heard, Job Dekker, and Emmanuel Barillot. 2015. “HiC-Pro: An Optimized and Flexible Pipeline for Hi-C Data Processing.” *Genome Biology* 16 (December): 259.

Sexton, T., E. Yaffe, E. Kenigsberg, F. Bantignies, B. Leblanc, M. Hoichman, H. Parrinello, A. Tanay, and G. Cavalli. 2012. “Three-Dimensional Folding and Functional Organization Principles of the Drosophila Genome.” *Cell* 148 (3): 458–72.

Sharma, Rahul, Daniel Jost, Jop Kind, Georgina Gómez-Saldivar, Bas van Steensel, Peter Askjaer, Cédric Vaillant, and Peter Meister. 2014. “Differential Spatial and Structural Organization of the X Chromosome Underlies Dosage Compensation in C. Elegans.” *Genes & Development* 28 (23): 2591–96.

Sharma, Rahul, and Peter Meister. 2013. “Nuclear Organization in the Nematode C. Elegans.” *Current Opinion in Cell Biology* 25 (3): 395–402.

Singh, R. N., and J. E. Sulston. 1978. “Some Observations On Moulting in Caenorhabditis Elegans.” *Nematologica* 24 (1): 63–71.

Stear, Jeffrey H., and Mark B. Roth. 2002. “Characterization of HCP-6, a C. Elegans Protein Required to Prevent Chromosome Twisting and Merotelic Attachment.” *Genes & Development* 16 (12): 1498–1508.

Steiner, Florian A., and Steven Henikoff. 2014. “Holocentromeres Are Dispersed Point Centromeres Localized at Transcription Factor Hotspots.” *eLife* 3 (January): e02025.

Stevens, Tim J., David Lando, Srinjan Basu, Liam P. Atkinson, Yang Cao, Steven F. Lee, Martin Leeb, et al. 2017. “3D Structures of Individual Mammalian Genomes Studied by Single-Cell Hi-C.” *Nature* 544 (7648): 59–64.

Stroustrup, Nicholas, Bryne E. Ulmschneider, Zachary M. Nash, Isaac F. López-Moyado, Javier Apfeld, and Walter Fontana. 2013. “The Caenorhabditis Elegans Lifespan Machine.” *Nature Methods* 10 (7): 665–70.

Sulston, J. E., and H. R. Horvitz. 1977. “Post-Embryonic Cell Lineages of the Nematode, Caenorhabditis Elegans.” *Developmental Biology* 56 (1): 110–56.

Towbin, Benjamin D., Cristina González-Aguilera, Ragna Sack, Dimos Gaidatzis, Véronique

Kalck, Peter Meister, Peter Askjaer, and Susan M. Gasser. 2012. “Step-Wise Methylation of Histone H3K9 Positions Heterochromatin at the Nuclear Periphery.” *Cell* 150 (5): 934–47.

Uhlmann, F., F. Lottspeich, and K. Nasmyth. 1999. “Sister-Chromatid Separation at Anaphase Onset Is Promoted by Cleavage of the Cohesin Subunit Scc1.” *Nature* 400 (6739): 37–42.

Venev, Sergey, Nezar Abdennur, Anton Goloborodko, Ilya Flyamer, Geoffrey Fudenberg, Johannes Nuebler, Aleksandra Galitsyna, et al. 2021. *open2c/cooltools: v0.4.1*. https://doi.org/10.5281/zenodo.5214125.

Walther, Nike, M. Julius Hossain, Antonio Z. Politi, Birgit Koch, Moritz Kueblbeck, Øyvind Ødegård-Fougner, Marko Lampe, and Jan Ellenberg. 2018. "A Quantitative Map of Human Condensins Provides New Insights into Mitotic Chromosome Architecture." *The Journal of Cell Biology* 217 (7): 2309–28.

Wang, Fang, John Yoder, Igor Antoshechkin, and Min Han. 2003. "Caenorhabditis Elegans EVL-14/PDS-5 and SCC-3 Are Essential for Sister Chromatid Cohesion in Meiosis and Mitosis." *Molecular and Cellular Biology* 23 (21): 7698–7707.

Weide, Robin H. van der, Teun van den Brand, Judith H. I. Haarhuis, Hans Teunissen, Benjamin D. Rowland, and Elzo de Wit. 2021. "Hi-C Analyses with GENOVA: A Case Study with Cohesin Variants." *NAR Genomics and Bioinformatics* 3 (2): lqab040.

Wutz, Gordana, Rene Ladurner, Brian Glenn St Hilaire, Roman R. Stocsits, Kota Nagasaka, Benoit Pignard, Adrian Sanborn, et al. 2020. "ESCO1 and CTCF Enable Formation of Long Chromatin Loops by Protecting cohesinSTAG1 from WAPL." *eLife* 9 (February). https://doi.org/10.7554/eLife.52091.

Wutz, Gordana, Csilla Várnai, Kota Nagasaka, David A. Cisneros, Roman R. Stocsits, Wen Tang, Stefan Schoenfelder, et al. 2017. "Topologically Associating Domains and Chromatin Loops Depend on Cohesin and Are Regulated by CTCF, WAPL, and PDS5 Proteins." *The EMBO Journal* 36 (24): 3573–99.

Yatskevich, Stanislau, James Rhodes, and Kim Nasmyth. 2019. "Organization of Chromosomal DNA by SMC Complexes." *Annual Review of Genetics* 53 (December): 445–82.

Yonker, Stephanie A., and Barbara J. Meyer. 2003. "Recruitment of C. Elegans Dosage Compensation Proteins for Gene-Specific versus Chromosome-Wide Repression." *Development* 130 (26): 6519–32.

Zuin, Jessica, Gregory Roth, Yinxiu Zhan, Julie Cramard, Josef Redolfi, Ewa Piskadlo, Pia Mach, et al. 2021. "Nonlinear Control of Transcription through Enhancer-Promoter Interactions." *bioRxiv*. https://doi.org/10.1101/2021.04.22.440891.